Supporting Information

to the manuscript:

Probing naphthalene diimide and 3-hydroxypropylphosphate as end-conjugating moieties for improved thrombin binding aptamers: structural and biological effects

Claudia Riccardi,[1] Kévan Pérez de Carvasal,[2], Chiara Platella,[1] Albert Meyer,[2] Michael Smietana,[2] François Morvan,[2,*] Daniela Montesarchio[1,*]

[1]*Department of Chemical Sciences, University of Naples Federico II, 80126 Naples, Italy*

[2]*Institut des Biomolécules Max Mousseron, Université de Montpellier, CNRS, ENSCM, 34095 Montpellier, France*

*Corresponding authors. E-mail addresses:
francois.morvan@umontpellier.fr (F. Morvan); daniela.montesarchio@unina.it (D. Montesarchio)

Table of contents:

Synthesis and characterization of 4,4′-dimethoxytrityl-NDI-propyl-diisopropyl phosphoramidite 6:

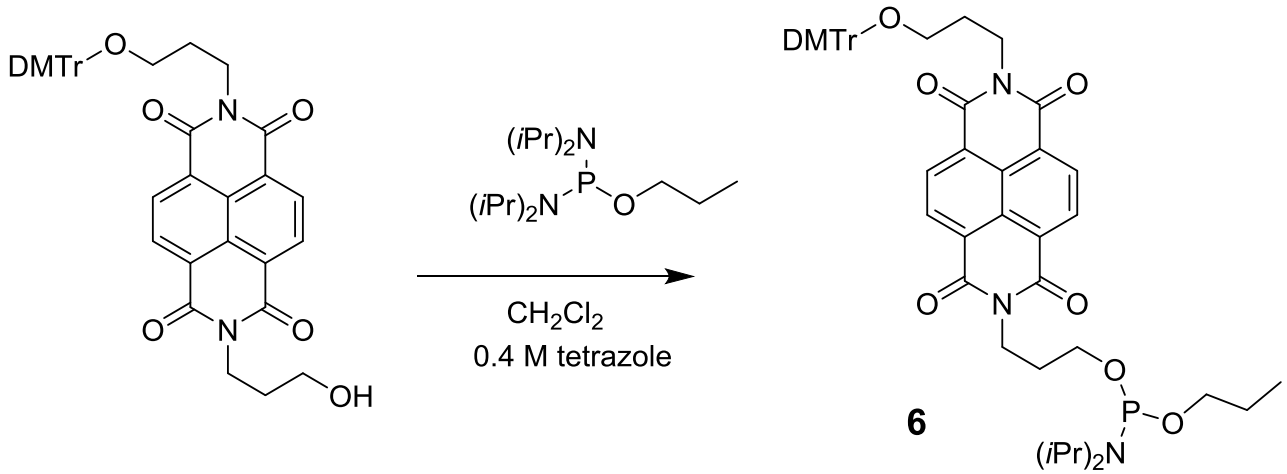

To a solution of 4,4′-dimethoxytrityl-NDI (100 mg, 0.146 mmol) in dry CH_2Cl_2 (4 mL) was added bis(diisopropylamino)propyloxyphosphine (42 mg, 0.146 mmol) and 0.4 M tetrazole in dry acetonitrile (182 µL, 0.073 mmol). The reaction was monitored by TLC (cyclohexane/AcOEt/NEt_3 5:4:1, v/v:v), after 1 h, the reaction was quenched by addition of 5 mL of brine. The reaction mixture was extracted with CH_2Cl_2, then the organic phase was dried over anhydrous Na_2SO_4, filtered, and concentrated under vacuum. Compound **6** was purified by silica gel column chromatography eluting with a solution of cyclohexane/AcOEt, 8:2 v/v, containing 4% of NEt_3. 70 mg of pure compound **6** were thus obtained (0.08 mmol, 55 %).

^{1}H NMR (400 MHz, $CDCl_3$): δ (ppm) 8.73-8.69 (m, 4H, H-NDI), 7.11-7.35 (m, 9H, H-Dmtr), 6.66 (d, J = 8.9 Hz, 4H, H-Dmtr), 4.34 (td, 4H, -N-CH_2-), 3.73-3.84 (m, 8H, PO-CH_2-, -OCH_3), 3.49-3.60 (m, 4H, -CH-, PO-CH_2-), 3.22 (t, J = 5.7 Hz, 2H, -CH_2-O-Dmtr), 2.06-2.13 (m, 4H, -CH_2-), 1.54-1.64 (m, 4H, -CH_2-), 1.16 (dd, J = 7.7 Hz, J = 6.8 Hz, 12H, CH_3 isoprop), 0.90 (t, J = 7.4 Hz, 3H, CH_3).

^{13}C NMR (100 MHz, $CDCl_3$): 163.0, 158.4, 144.8, 136.4,130.9, 130.9, 130.0, 128.3, 127.8, 126.9, 126.8,126.7, 113.0, 86.2, 65.3, 65.2, 62.2, 61.7, 61.5, 55.28, 43.0, 42.9, 39.3, 38.8, 30.1, 30.0, 28.5, 24.8, 24.8, 24.7, 10.7.

^{31}P NMR (100 MHz, $CDCl_3$): 145.7. HR-ESI-QToF MS (positive mode): m/z calcd for $C_{50}H_{59}N_3O_9P$ $[M+H]^+$: 892.3933 found 892.3942.

^{1}H, $^{13}C\{^{1}H\}$ and $^{31}P\{^{1}H\}$-NMR spectra of 6 in $CDCl_3$:

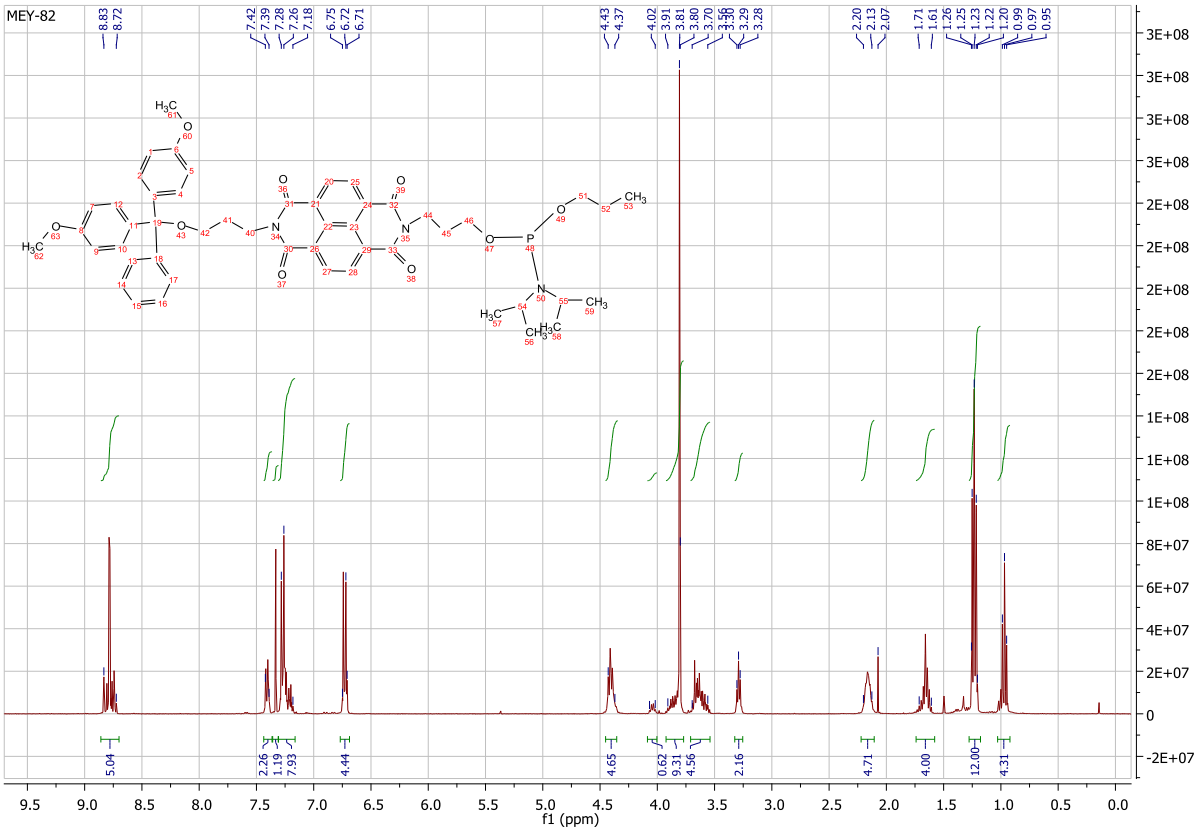

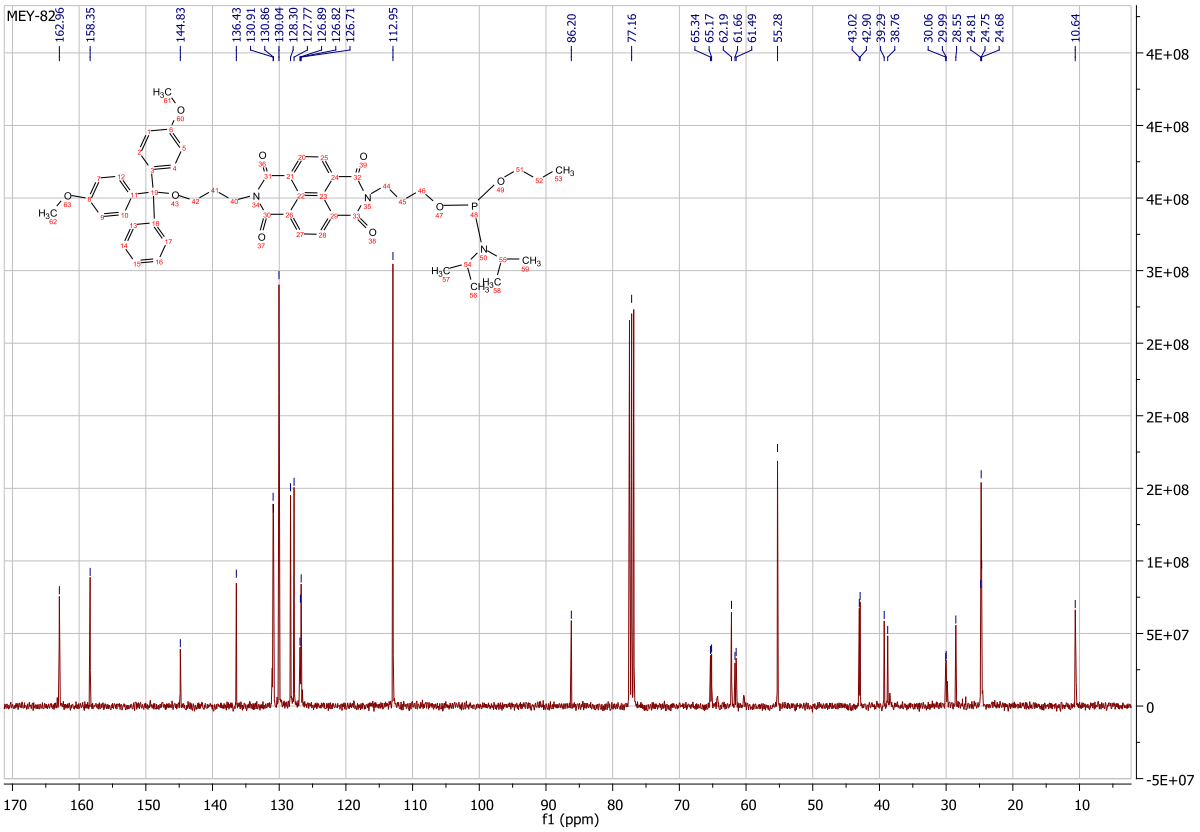

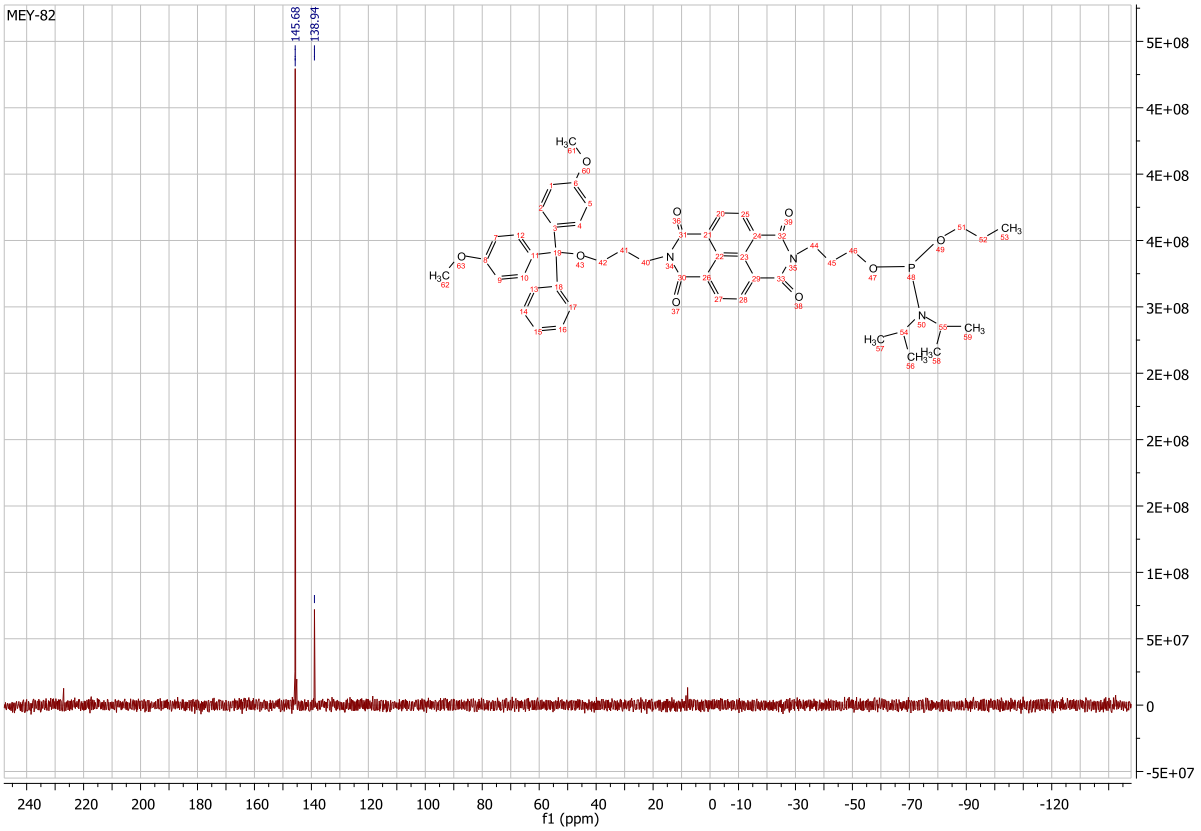
MEY-82
145.68
138.94
5E+08
4E+08
4E+08
4E+08
3E+08
2E+08
2E+08
2E+08
1E+08
5E+07
0
-5E+07
240
220
200
180
160
140
120
100
80
60
40
20
0
-10
-30
-50
-70
-90
-120
f1 (ppm)

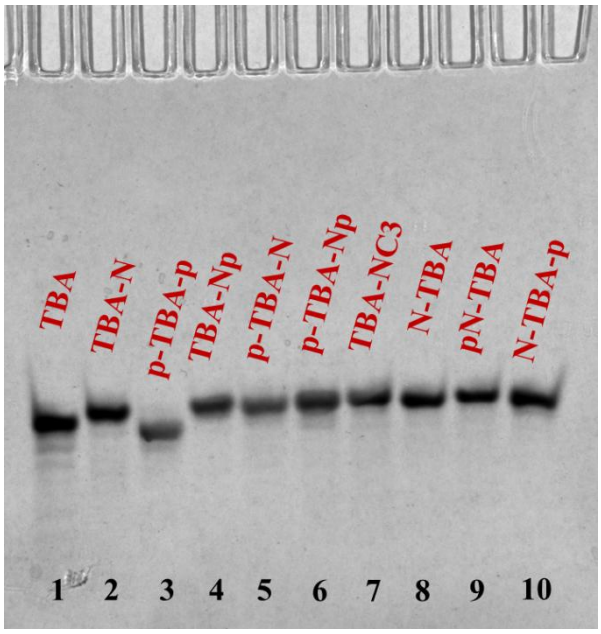

Figure S1. Representative 20% denaturing polyacrylamide gel electrophoresis (8 M urea) at 10.5 μM sample concentration, run at constant 200 V at r.t. for 2.5 h in TBE 1X as running buffer. Lane 1: **TBA**; lane 2: **TBA-N**; lane 3: **p-TBA-p**; lane 4: **TBA-Np**; lane 5: **p-TBA-N**; lane 6: **p-TBA-Np**; lane 7: **TBA-NC3**; lane 8: **N-TBA**; lane 9: **pN-TBA**; lane 10: **N-TBA-p**.

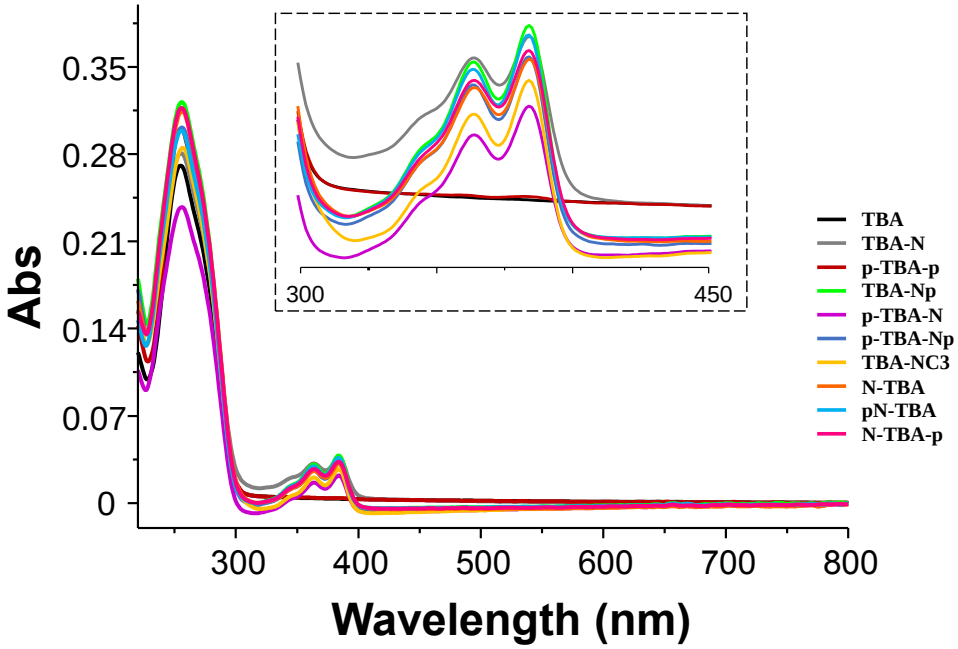

Figure S2. Overlapped UV-vis spectra of the investigated TBA derivatives in comparison with unmodified TBA and TBA-N, used as reference sequences. All the investigated oligonucleotides were analyzed at 2 μM concentration in H_2O at r.t. The inset shows an enlargement of the 300-600 nm region of the spectra, to better highlight the characteristic UV-vis contribution of the NDI group.

Aptamer	TDS factors					
	K^+-rich buffer			Na^+-rich buffer		
	$\Delta A_{240}/\Delta A_{295}$	$\Delta A_{255}/\Delta A_{295}$	$\Delta A_{275}/\Delta A_{295}$	$\Delta A_{240}/\Delta A_{295}$	$\Delta A_{255}/\Delta A_{295}$	$\Delta A_{275}/\Delta A_{295}$
TBA	**0.7**	**0.1**	**0.6**	**1.0**	**0.6**	**1.5**
TBA-N	**1.2**	**0.6**	**1.8**	**0.8**	**0.5**	**1.3**
p-TBA-p	**1.0**	**0.1**	**0.8**	**0.5**	**0.1**	**0.9**
TBA-Np	**0.2**	**0.2**	**0.6**	**0.8**	**0.4**	**1.2**
p-TBA-N	**0.5**	**0.1**	**0.7**	**0.6**	**0.1**	**1.0**
p-TBA-Np	**0.6**	**0.2**	**0.9**	**0.9**	**0.5**	**1.4**
TBA-NC3	**0.2**	**0.3**	**0.5**	**0.9**	**0.4**	**1.2**
N-TBA	**0.5**	**0.1**	**0.5**	**0.6**	**0.1**	**0.5**
pN-TBA	**0.5**	**0.1**	**0.5**	**1.0**	**0.4**	**1.0**
N-TBA-p	**0.9**	**0.3**	**0.9**	**0.8**	**0.1**	**0.8**

Table S1. Ratios between values at different absorbance wavelengths as calculated from normalized TDS spectra for all the studied oligonucleotides in both the selected phosphate buffer solutions, according to literature protocols.[1]

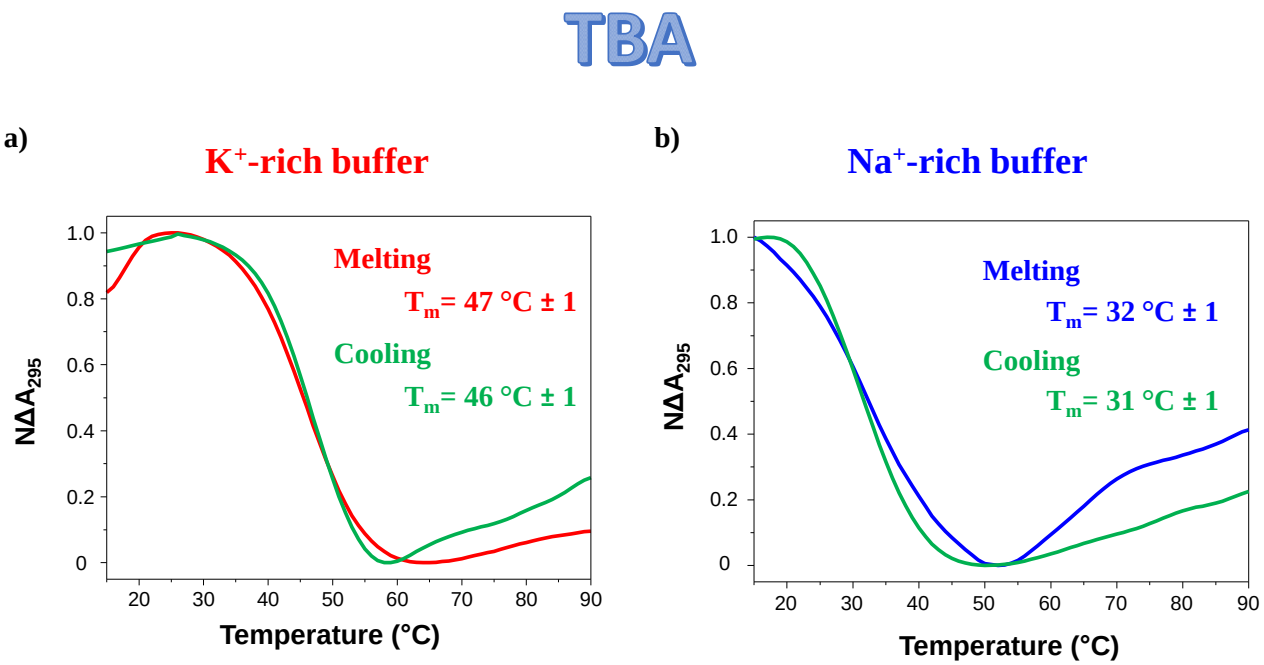

Figure S3. Representative normalized UV-melting and UV-cooling profiles of **TBA** at 2 µM concentration in both the selected K^+- (**a**) and Na^+-rich (**b**) buffer solutions. The UV-monitored thermal curves were recorded following the signal at 295 nm in both saline conditions, with a temperature scan rate of 1 °C/min.

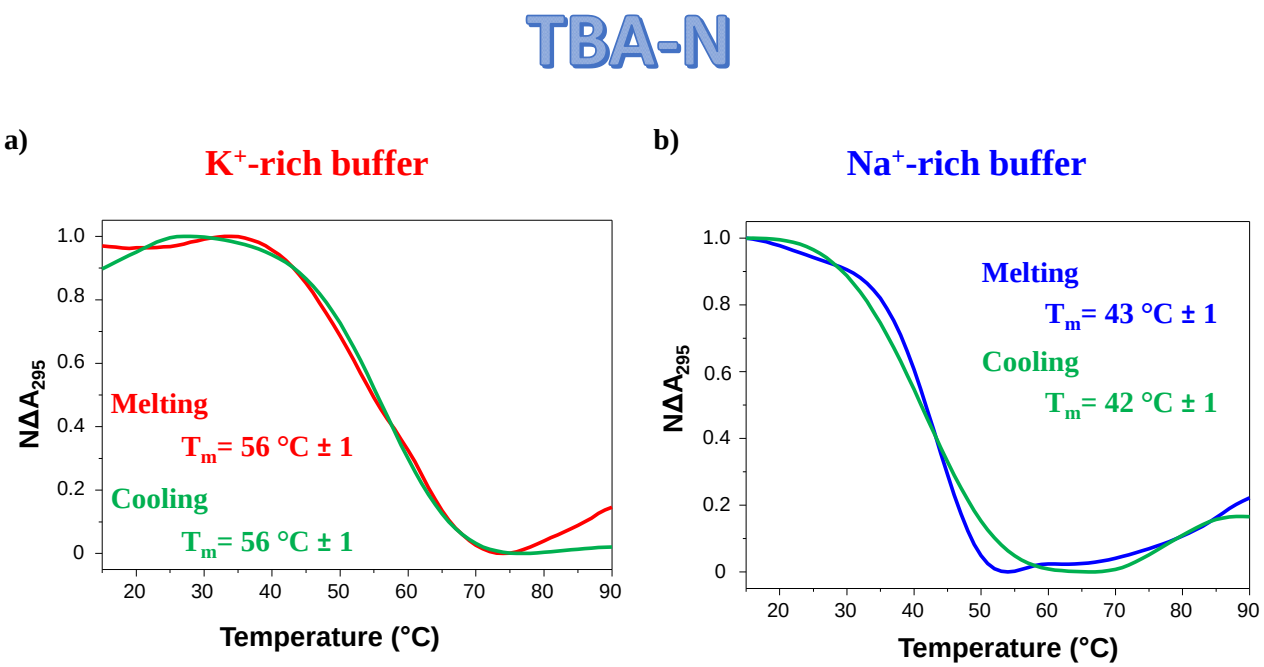

Figure S4. Representative normalized UV-melting and UV-cooling profiles of **TBA-N** at 2 µM concentration in both the selected K^+- (**a**) and Na^+-rich (**b**) buffer solutions. The UV-monitored thermal curves were recorded following the signal at 295 nm in both saline conditions, with a temperature scan rate of 1 °C/min.

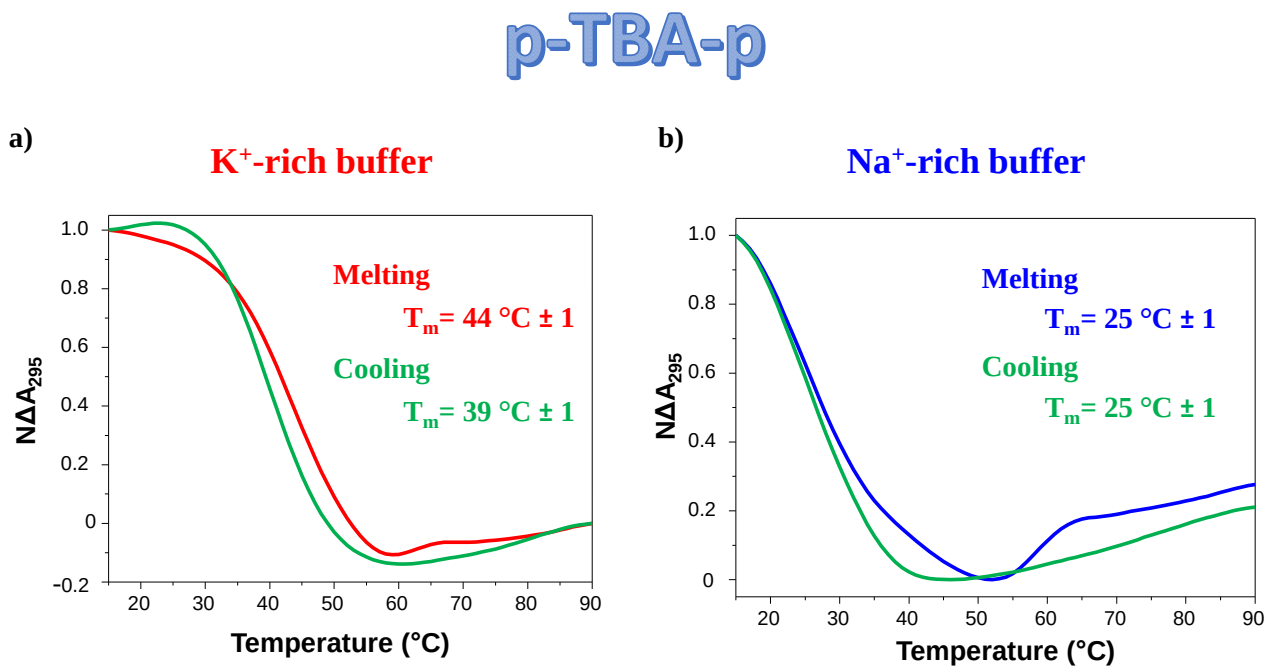

Figure S5. Representative normalized UV-melting and UV-cooling profiles of **p-TBA-p** at 2 µM concentration in both the selected K^+- (**a**) and Na^+-rich (**b**) buffer solutions. The UV-monitored thermal curves were recorded following the signal at 295 nm in both saline conditions, with a temperature scan rate of 1 °C/min.

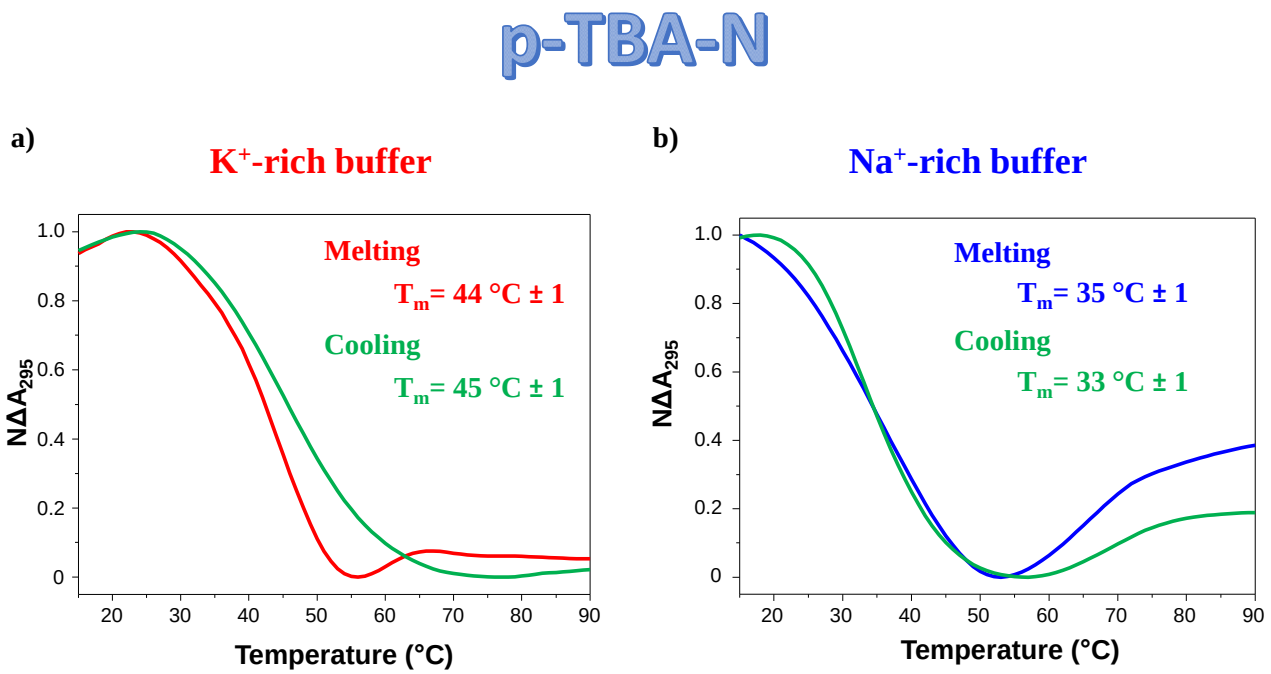

Figure S6. Representative normalized UV-melting and UV-cooling profiles of **p-TBA-N** at 2 µM concentration in both the selected K^+- (**a**) and Na^+-rich (**b**) buffer solutions. The UV-monitored thermal curves were recorded following the signal at 295 nm in both saline conditions, with a temperature scan rate of 1 °C/min.

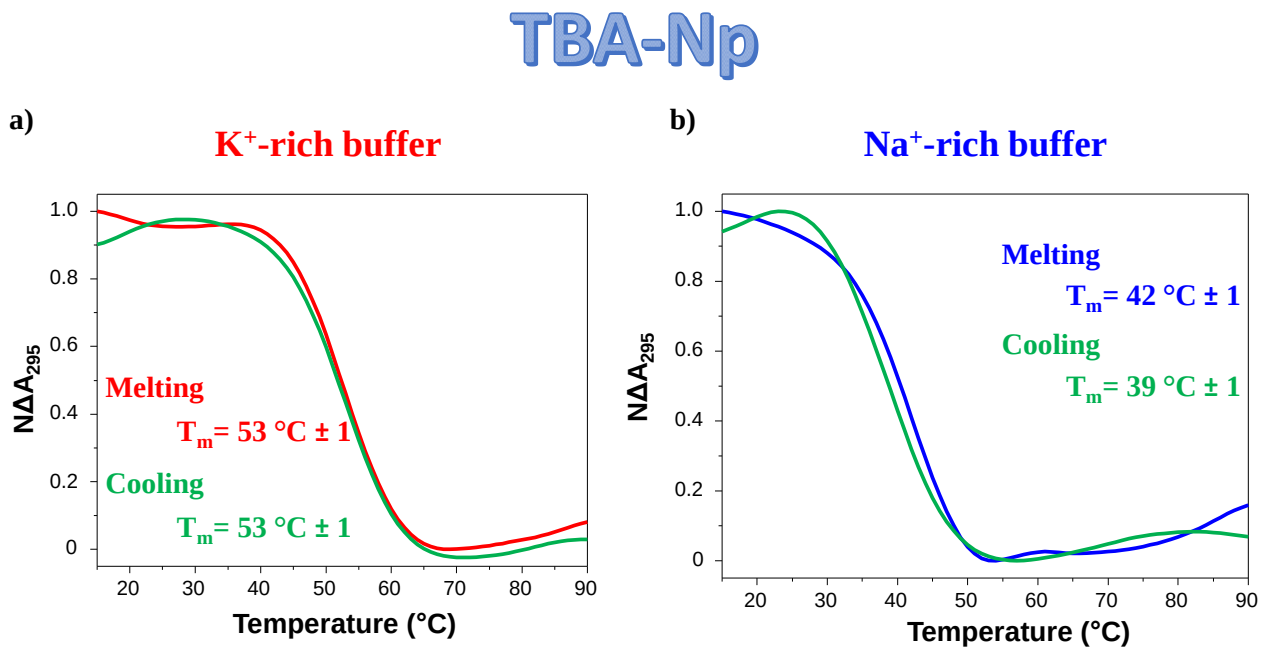

Figure S7. Representative normalized UV-melting and UV-cooling profiles of **TBA-Np** at 2 µM concentration in both the selected K^+- (**a**) and Na^+-rich (**b**) buffer solutions. The UV-monitored thermal curves were recorded following the signal at 295 nm in both saline conditions, with a temperature scan rate of 1 °C/min.

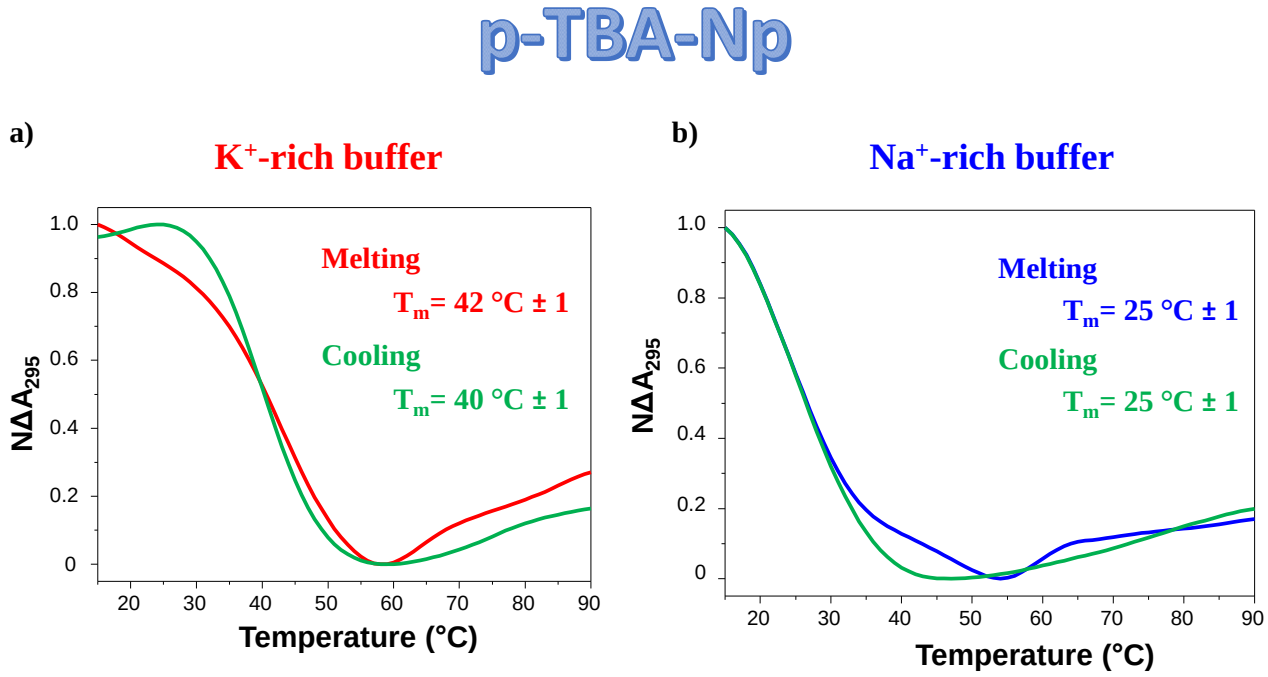

Figure S8. Representative normalized UV-melting and UV-cooling profiles of **p-TBA-Np** at 2 µM concentration in both the selected K^+- (**a**) and Na^+-rich (**b**) buffer solutions. The UV-monitored thermal curves were recorded following the signal at 295 nm in both saline conditions, with a temperature scan rate of 1 °C/min.

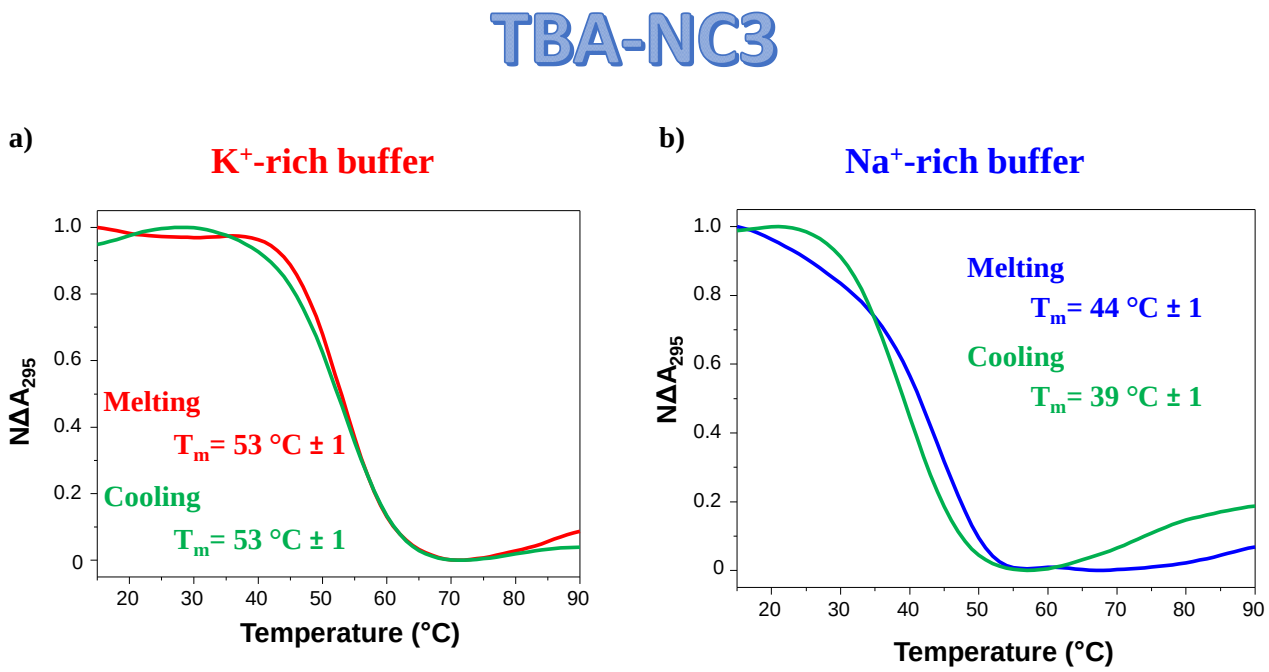

Figure S9. Representative normalized UV-melting and UV-cooling profiles of **TBA-NC3** at 2 µM concentration in both the selected K^+- (**a**) and Na^+-rich (**b**) buffer solutions. The UV-monitored thermal curves were recorded following the signal at 295 nm in both saline conditions, with a temperature scan rate of 1 °C/min.

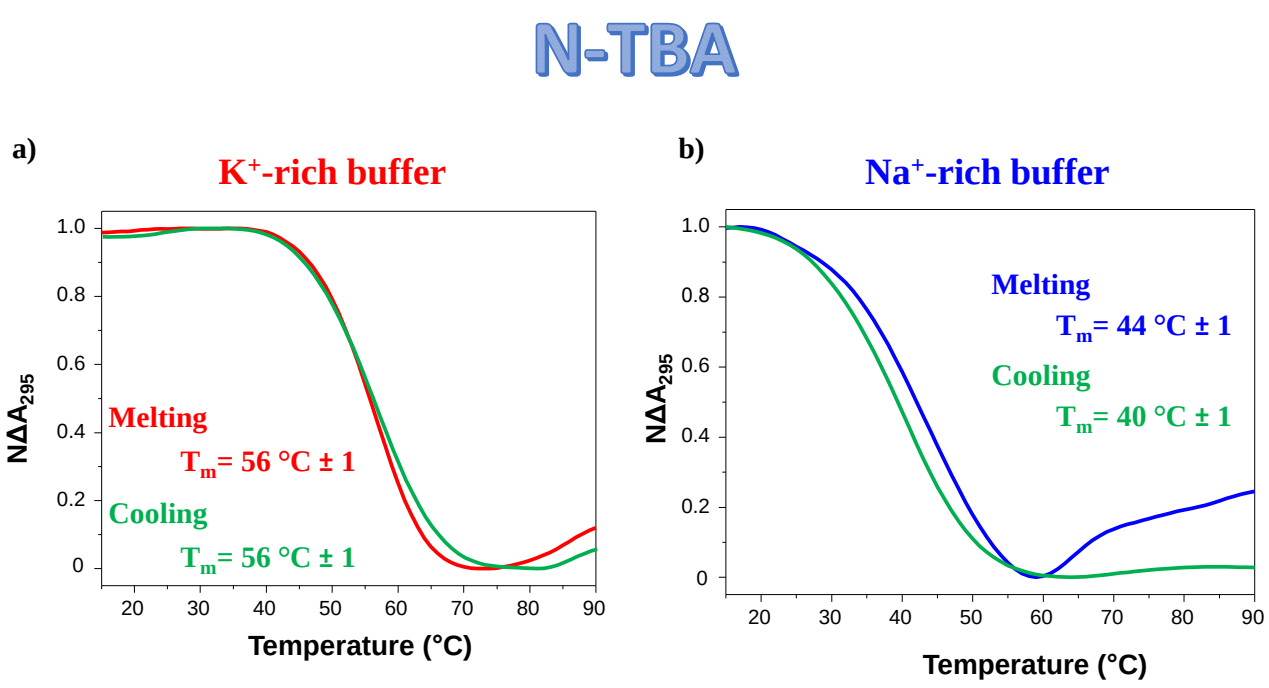

Figure S10. Representative normalized UV-melting and UV-cooling profiles of **N-TBA** at 2 µM concentration in both the selected K^+- (**a**) and Na^+-rich (**b**) buffer solutions. The UV-monitored thermal curves were recorded following the signal at 295 nm in both saline conditions, with a temperature scan rate of 1 °C/min.

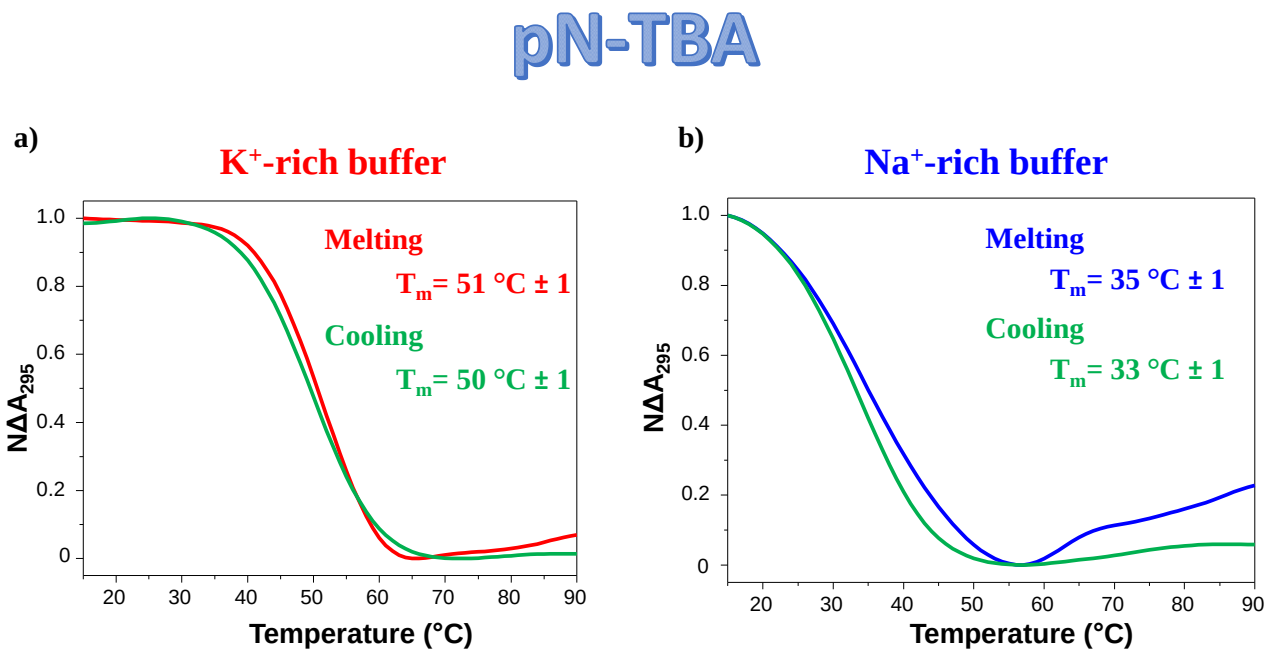

Figure S11. Representative normalized UV-melting and UV-cooling profiles of **pN-TBA** at 2 µM concentration in both the selected K^+- (**a**) and Na^+-rich (**b**) buffer solutions. The UV-monitored thermal curves were recorded following the signal at 295 nm in both saline conditions, with a temperature scan rate of 1 °C/min.

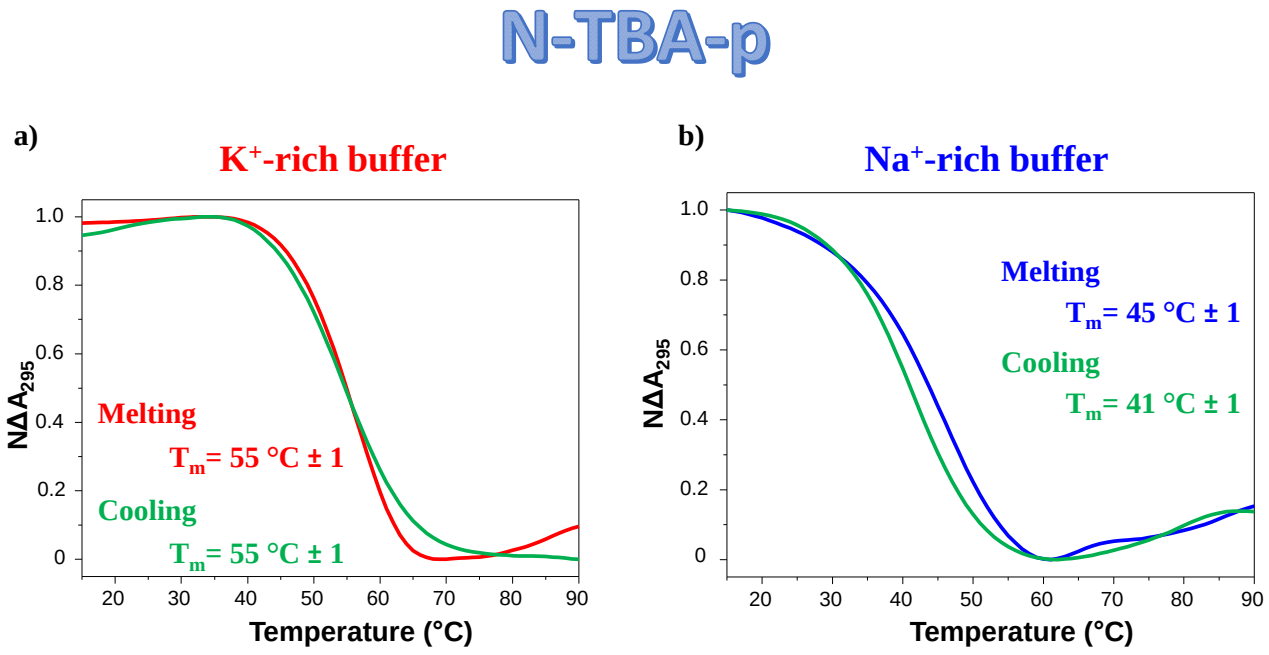

Figure S12. Representative normalized UV-melting and UV-cooling profiles of **N-TBA-p** at 2 µM concentration in both the selected K^+- (**a**) and Na^+-rich (**b**) buffer solutions. The UV-monitored thermal curves were recorded following the signal at 295 nm in both saline conditions, with a temperature scan rate of 1 °C/min.

Aptamer	UV-melting and cooling experiments					
	K^+-rich buffer			Na^+-rich buffer		
	Melting T_m (°C)	ΔT_m (°C)	Cooling T_m (°C)	Melting T_m (°C)	ΔT_m (°C)	Cooling T_m (°C)
TBA	47	-	46	32	-	31
TBA-N	56	+9	56	43	+11	42
p-TBA-p	44	-3	39	25	-7	25
TBA-Np	53	+6	53	42	+10	39
p-TBA-N	44	-3	45	35	+3	33
p-TBA-Np	42	-5	40	25	-7	25
TBA-NC3	53	+6	53	44	+12	39
N-TBA	56	+9	56	44	+12	40
pN-TBA	51	+4	50	35	+3	33
N-TBA-p	55	+8	55	45	+13	41

Table S2. Apparent melting temperature values obtained by UV-monitored thermal experiments at 295 nm for heating and cooling profiles of the here investigated oligonucleotides in the selected K^+- and Na^+-rich buffer solutions. Apparent T_m values were estimated using the method of the first derivative. The error associated with the T_m determination is ± 1 °C. ΔT_m is calculated by subtracting the measured T_m of unmodified TBA from that calculated for each modified TBA analogue.

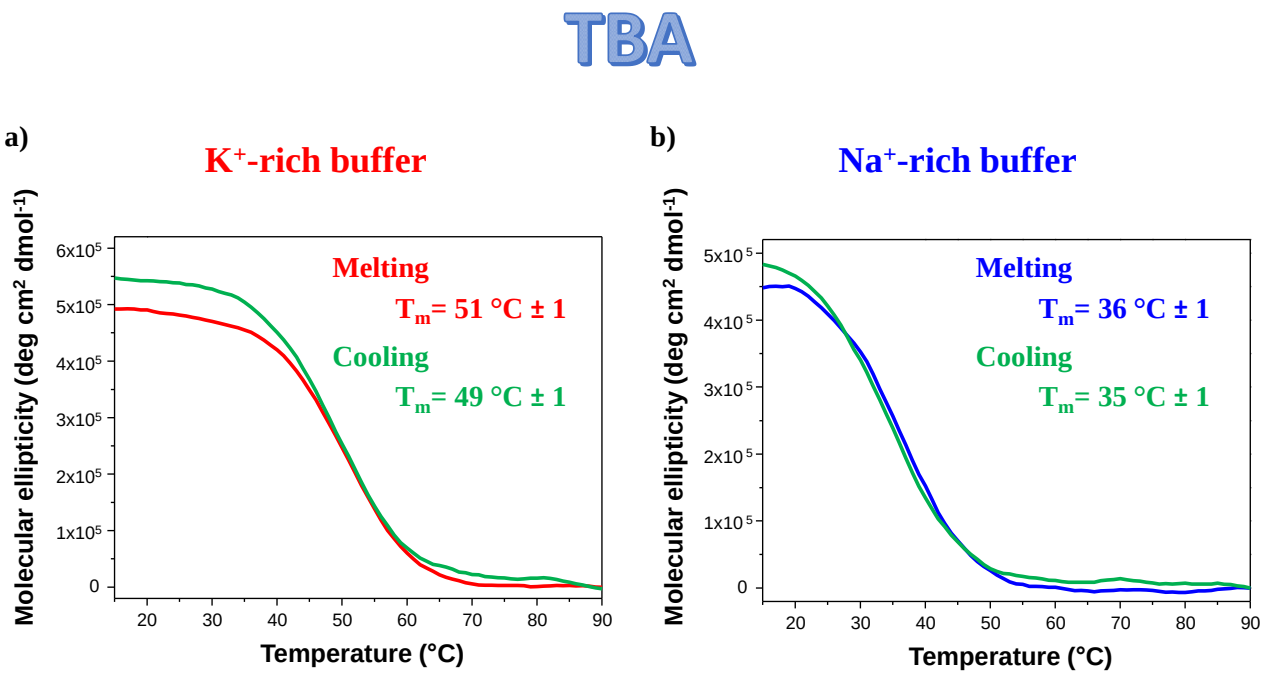

Figure S13. Representative CD-melting and CD-cooling profiles of **TBA** at 2 µM concentration in both the selected K^+- (**a**) and Na^+-rich (**b**) buffer solutions. The CD-monitored thermal curves were recorded following the signal at 295 nm in both saline conditions, with a temperature scan rate of 1 °C/min.

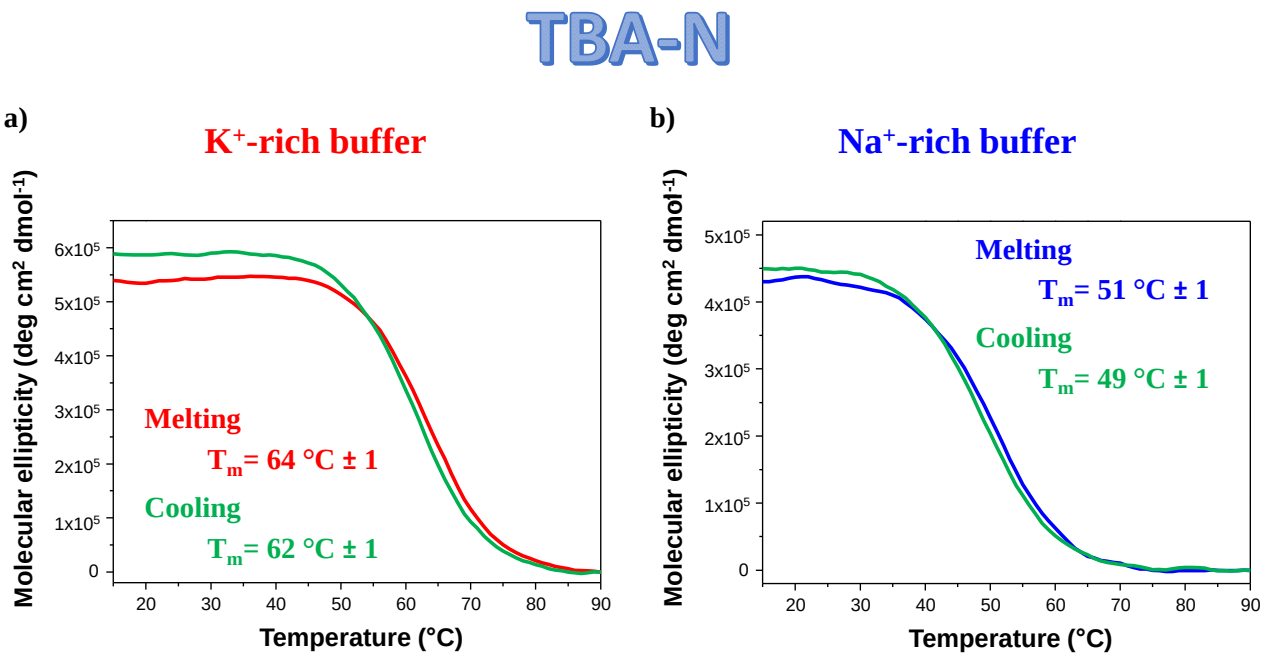

Figure S14. Representative CD-melting and CD-cooling profiles of **TBA-N** 2 µM concentration in both the selected K^+- (**a**) and Na^+-rich (**b**) buffer solutions. The CD-monitored thermal curves were recorded following the signal at 295 nm in both saline conditions, with a temperature scan rate of 1 °C/min.

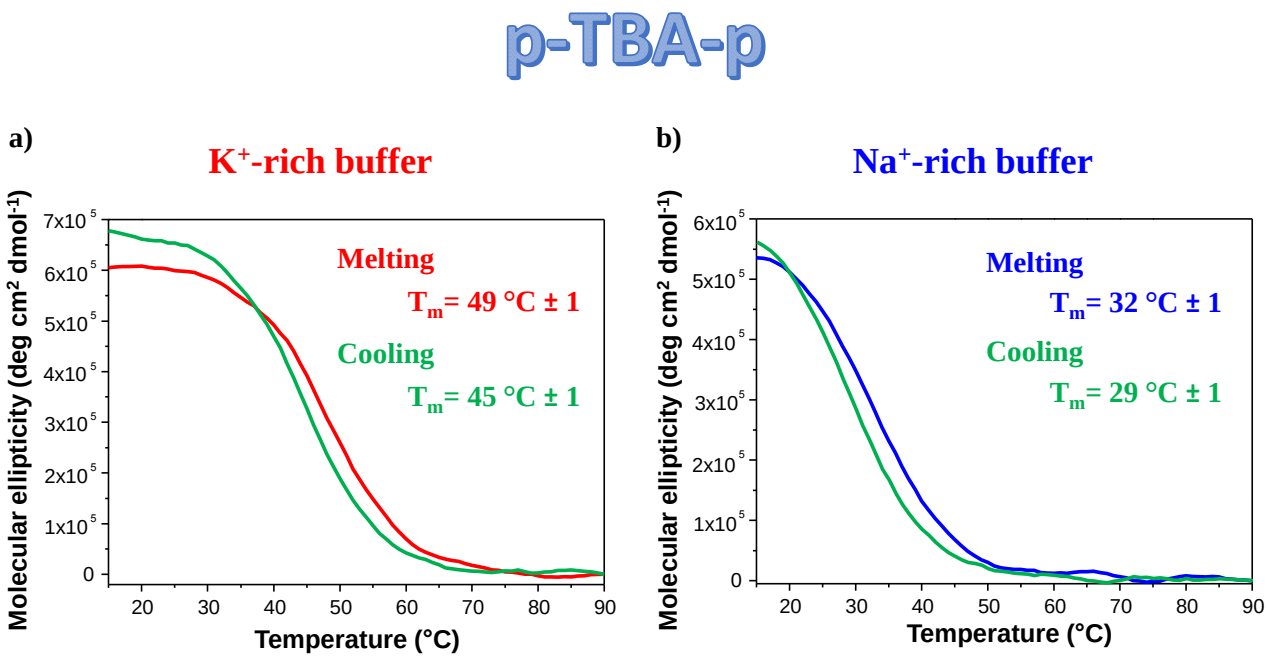

Figure S15. Representative CD-melting and CD-cooling profiles of the **p-TBA-p** at 2 µM concentration in both the selected K^+- (**a**) and Na^+-rich (**b**) buffer solutions. The CD-monitored thermal curves were recorded following the signal at 295 nm in both saline conditions, with a temperature scan rate of 1 °C/min.

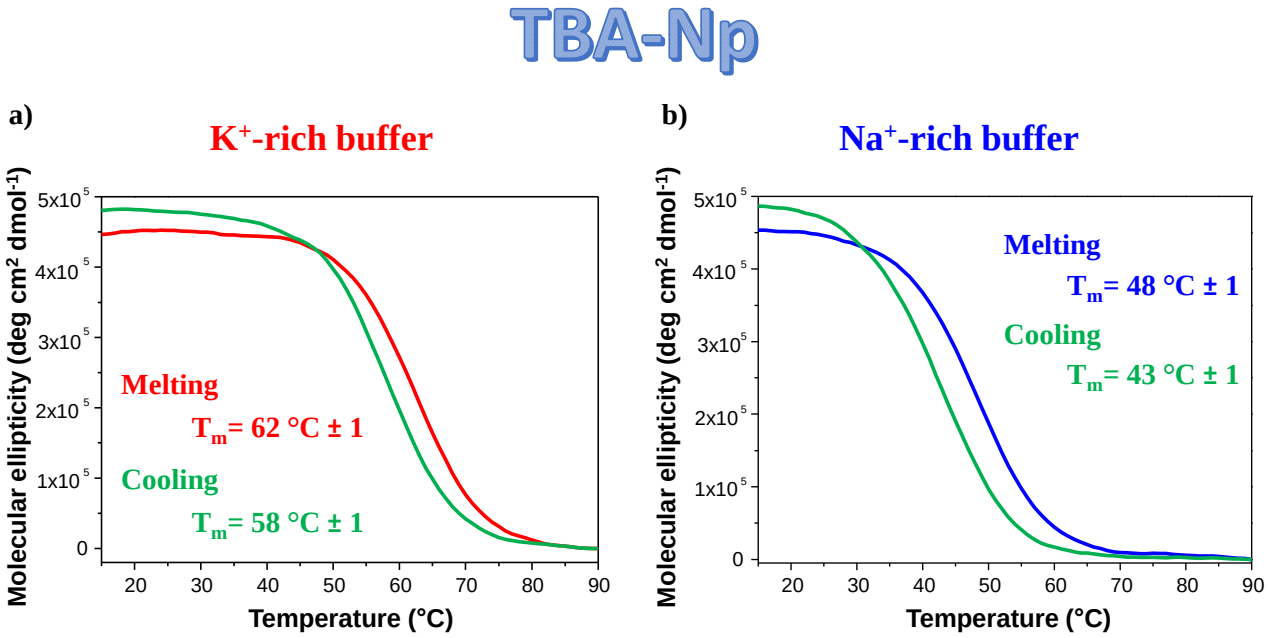

Figure S16. Representative CD-melting and CD-cooling profiles of the **TBA-Np** at 2 µM concentration in both the selected K^+- (**a**) and Na^+-rich (**b**) buffer solutions. The CD-monitored thermal curves were recorded following the signal at 295 nm in both saline conditions, with a temperature scan rate of 1 °C/min.

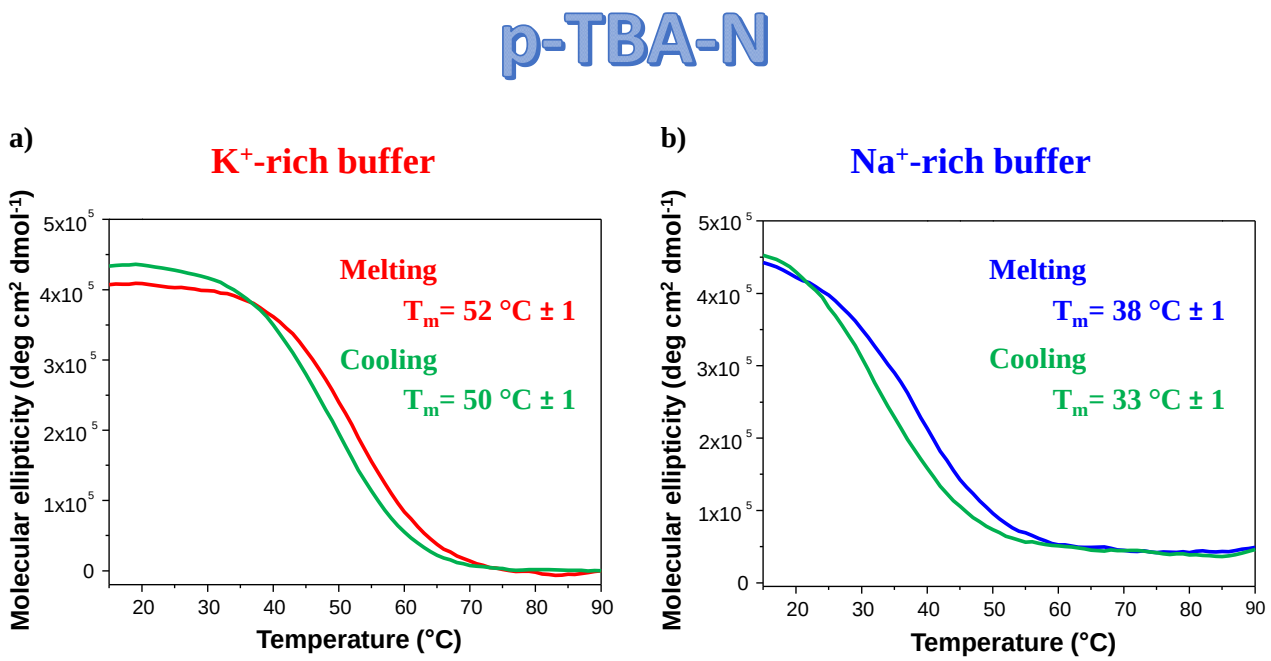

Figure S17. Representative CD-melting and CD-cooling profiles of the **p-TBA-N** at 2 µM concentration in both the selected K^+- (**a**) and Na^+-rich (**b**) buffer solutions. The CD-monitored thermal curves were recorded following the signal at 295 nm in both saline conditions, with a temperature scan rate of 1 °C/min.

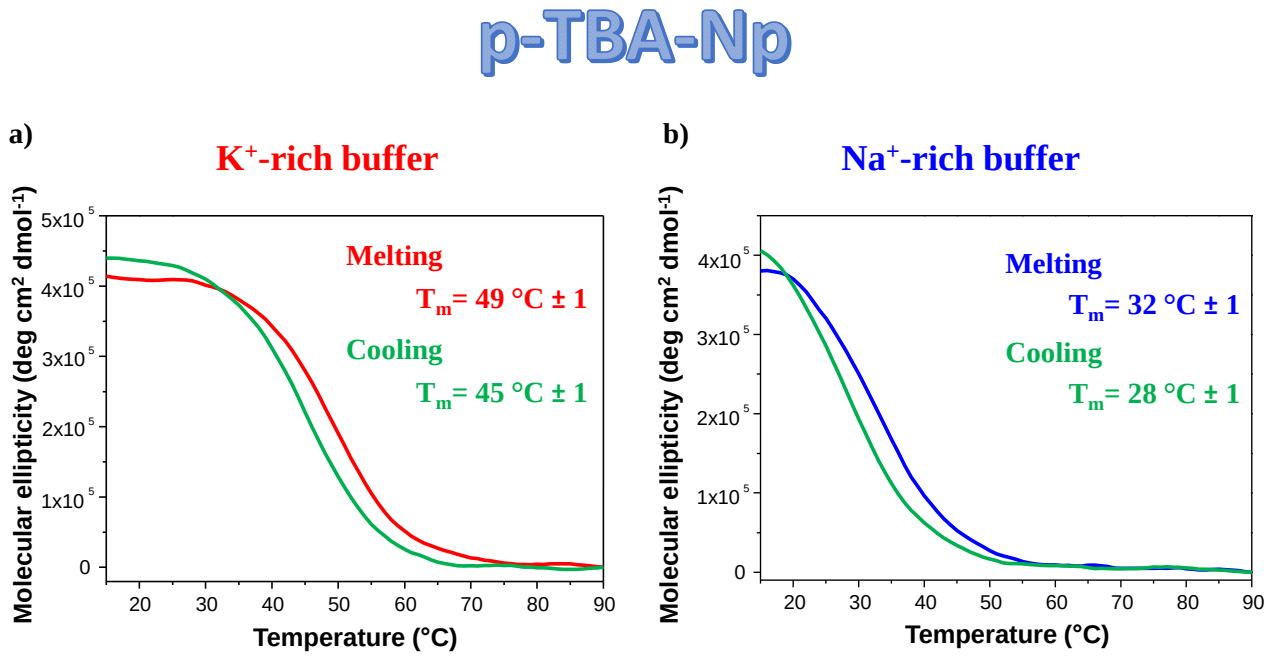

Figure S18. Representative CD-melting and CD-cooling profiles of the **p-TBA-Np** at 2 µM concentration in both the selected K^+- (**a**) and Na^+-rich (**b**) buffer solutions. The CD-monitored thermal curves were recorded following the signal at 295 nm in both saline conditions, with a temperature scan rate of 1 °C/min.

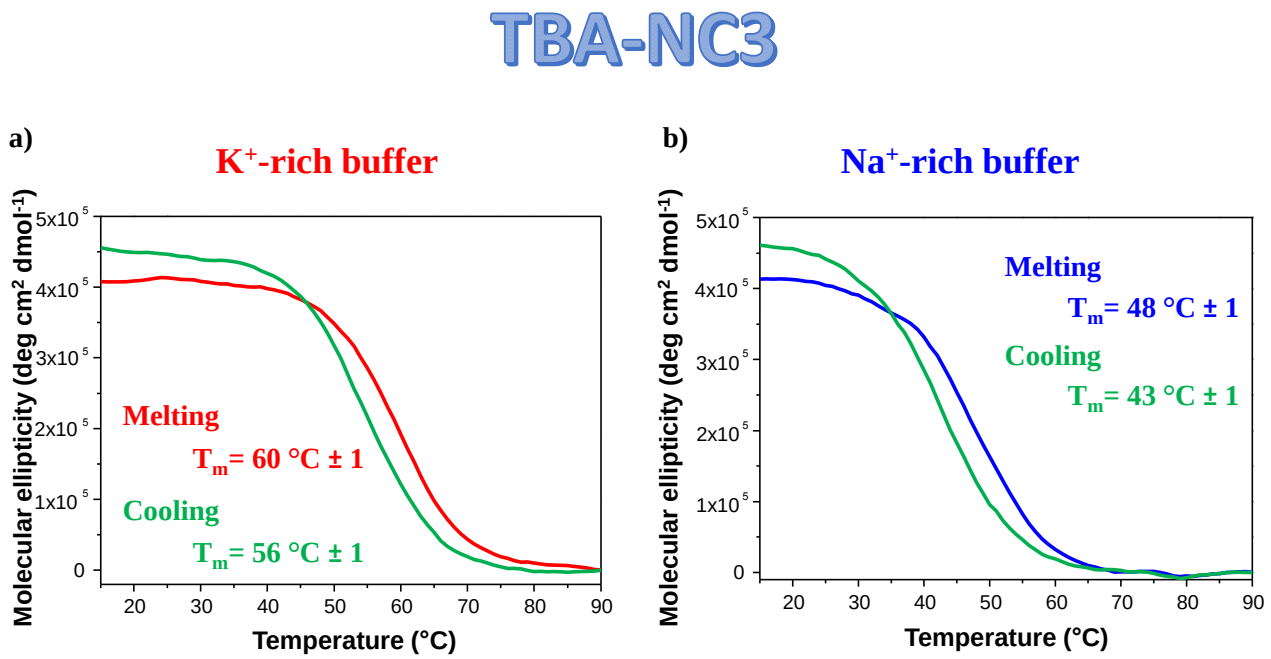

Figure S19. Representative CD-melting and CD-cooling profiles of the **TBA-NC3** at 2 µM concentration in both the selected K^+- (**a**) and Na^+-rich (**b**) buffer solutions. The CD-monitored thermal curves were recorded following the signal at 295 nm in both saline conditions, with a temperature scan rate of 1 °C/min.

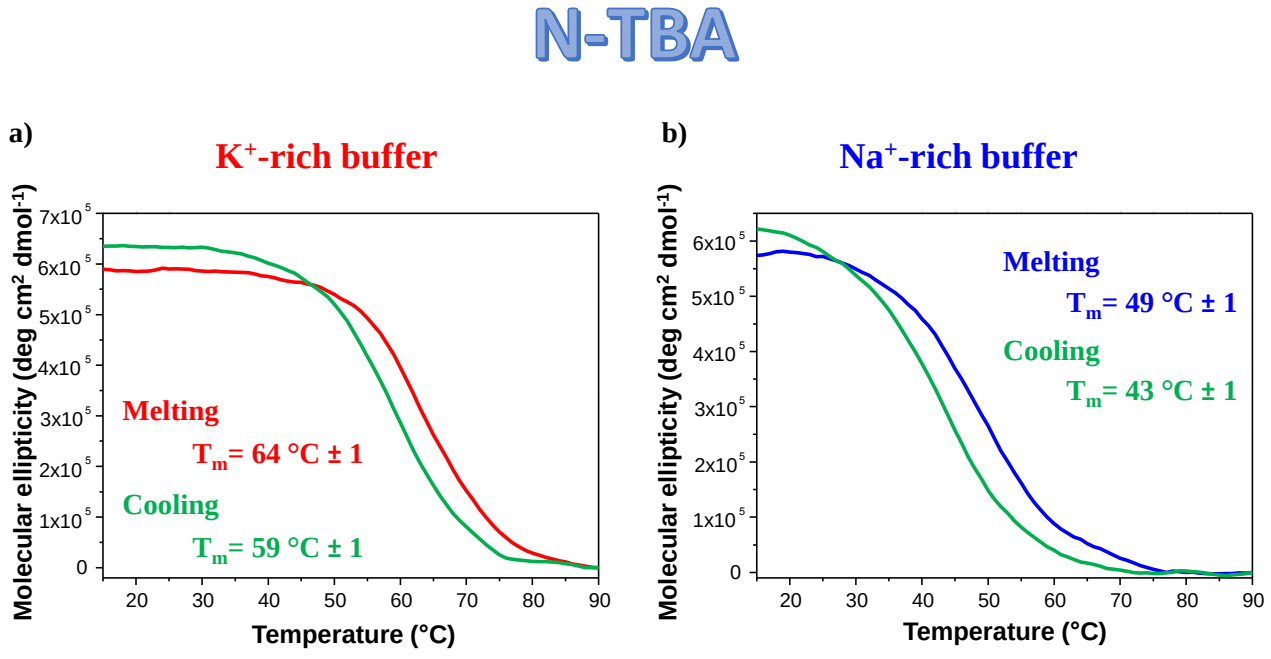

Figure S20. Representative CD-melting and CD-cooling profiles of the **N-TBA** at 2 µM concentration in both the selected K^+- (**a**) and Na^+-rich (**b**) buffer solutions. The CD-monitored thermal curves were recorded following the signal at 295 nm in both saline conditions, with a temperature scan rate of 1 °C/min.

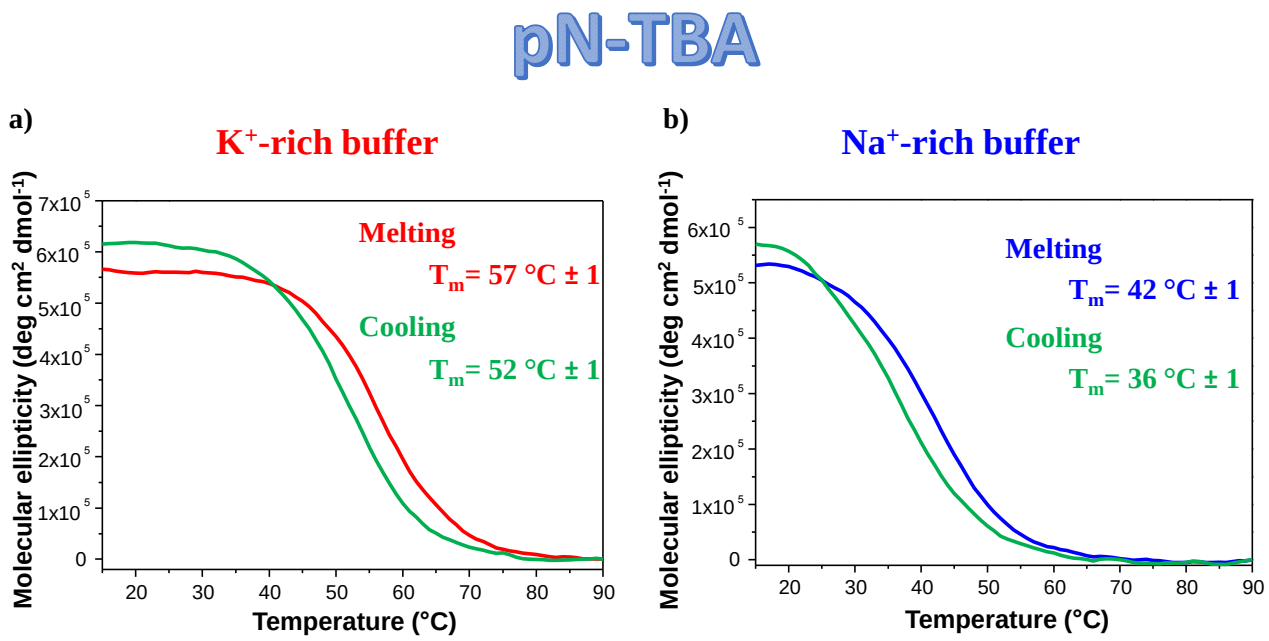

Figure S21. Representative CD-melting and CD-cooling profiles of the **pN-TBA** at 2 µM concentration in both the selected K^+- (**a**) and Na^+-rich (**b**) buffer solutions. The CD-monitored thermal curves were recorded following the signal at 295 nm in both saline conditions, with a temperature scan rate of 1 °C/min.

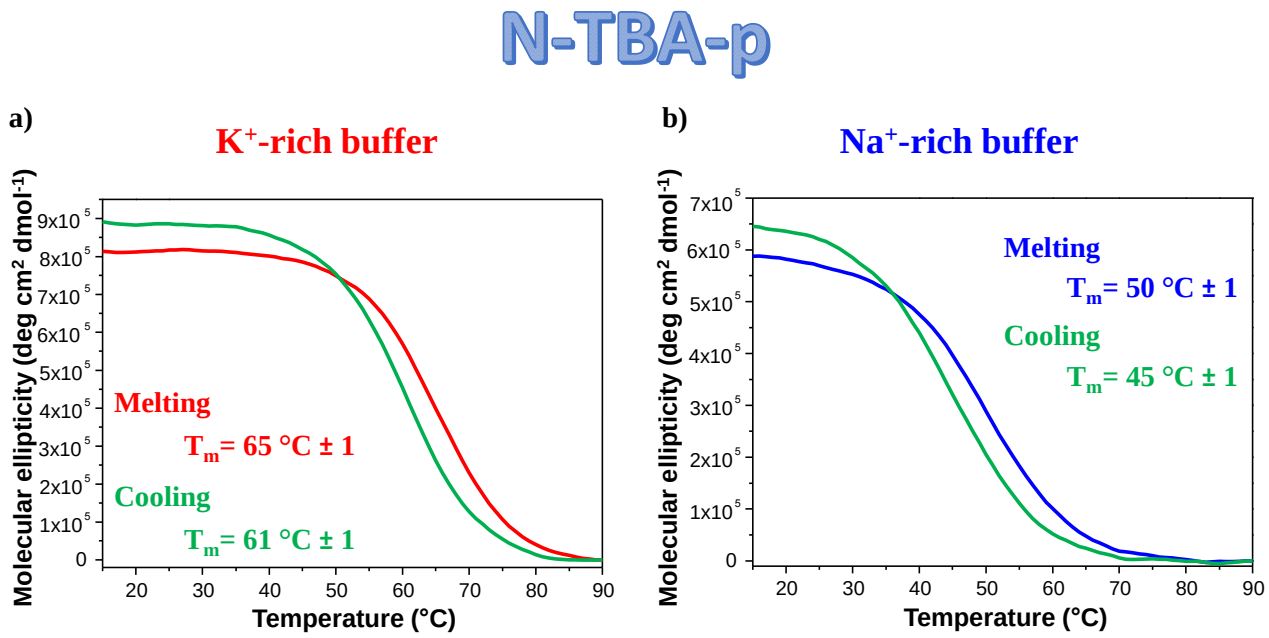

Figure S22. Representative CD-melting and CD-cooling profiles of the **N-TBA-p** at 2 µM concentration in both the selected K^+- (**a**) and Na^+-rich (**b**) buffer solutions. The CD-monitored thermal curves were recorded following the signal at 295 nm in both saline conditions, with a temperature scan rate of 1 °C/min.

CD thermal denaturation/renaturation measurements

More specifically, in the K^+-rich buffer (Figure 3c), **N-TBA-p, TBA-N**, **N-TBA**, **TBA-Np** and **TBA-NC3** gave the most stabilized G4 structures in the series, showing apparent T_m values respectively of 65, 64, 64, 62 and 60 °C, corresponding to ΔT_m of +14, +13, +13, +11 and +9 °C, compared to their natural counterpart. A T_m value of 57 °C – with ΔT_m of +6 °C with respect to the native aptamer – was found for **pN-TBA**, while **p-TBA-N** had the same thermal stability as the unmodified TBA. Conversely, CD analysis on **p-TBA-p** and **p-TBA-Np** analogues indicated a slight destabilization of their G4 structures with respect to unmodified TBA, with T_m values of 49 °C, i.e. 2 °C lower than their natural counterpart (Figures S13-S22 and Table S3).

A similar pattern was observed in the Na^+-rich medium (Figure 3d), with **TBA-N**, **N-TBA-p**, **N-TBA, TBA-Np** and **TBA-NC3** forming the most stable G4 structures, with apparent T_m values respectively of 51, 50, 49, 48 and 48 °C, corresponding to ΔT_m of +15, +14, +13, +12 and +12 °C compared to native TBA. Less stabilized G-quadruplex structures were formed by **pN-TBA** and **p-TBA-N**, exhibiting T_m values of 42 and 38 °C, i.e. 6 and 2 °C higher than unmodified TBA. Finally, **p-TBA-p** and **p-TBA-Np** proved to be the least stable analogues of the series, with ΔT_m of -4 °C with respect to unmodified TBA (Figures S13-S22 and Table S3).

Taken together, the CD-derived T_m values revealed this trend of G4 stability: **N-TBA-p** > **N-TBA** = **TBA-N** > **TBA-Np** > **TBA-NC3** > **pN-TBA** > **p-TBA-N** > TBA > **p-TBA-Np** > **p-TBA-p** in the K^+-rich buffer, and **TBA-N** > **N-TBA-p** > **N-TBA** > **TBA-Np** = **TBA-NC3** > **pN-TBA** > **p-TBA-N** > TBA > **p-TBA-p** > **p-TBA-Np** in the Na^+-rich buffer solution (Table S3).

Aptamer	CD-melting and cooling experiments					
	K^+-rich buffer			Na^+-rich buffer		
	Melting T_m (°C)	ΔT_m (°C)	Cooling T_m (°C)	Melting T_m (°C)	ΔT_m (°C)	Cooling T_m (°C)
TBA	51	-	49	36	-	35
TBA-N	64	+13	62	51	+15	49
p-TBA-p	49	-2	45	32	-4	29
TBA-Np	62	+11	58	48	+12	43
p-TBA-N	52	+1	50	38	+2	33
p-TBA-Np	49	-2	45	32	-4	28
TBA-NC3	60	+9	56	48	+12	43
N-TBA	64	+13	59	49	+13	43
pN-TBA	57	+6	52	42	+6	36
N-TBA-p	65	+14	61	50	+14	45

Table S3. Apparent melting temperature values obtained by CD-monitored thermal experiments for heating and cooling profiles of the here investigated oligonucleotides in the selected K^+- and Na^+-rich buffer solutions. Apparent T_m values were estimated from the maxima of the first derivative plots. The error associated with the T_m determination is ± 1 °C. ΔT_m is calculated by subtracting the measured T_m of unmodified TBA from that observed for each TBA analogue.

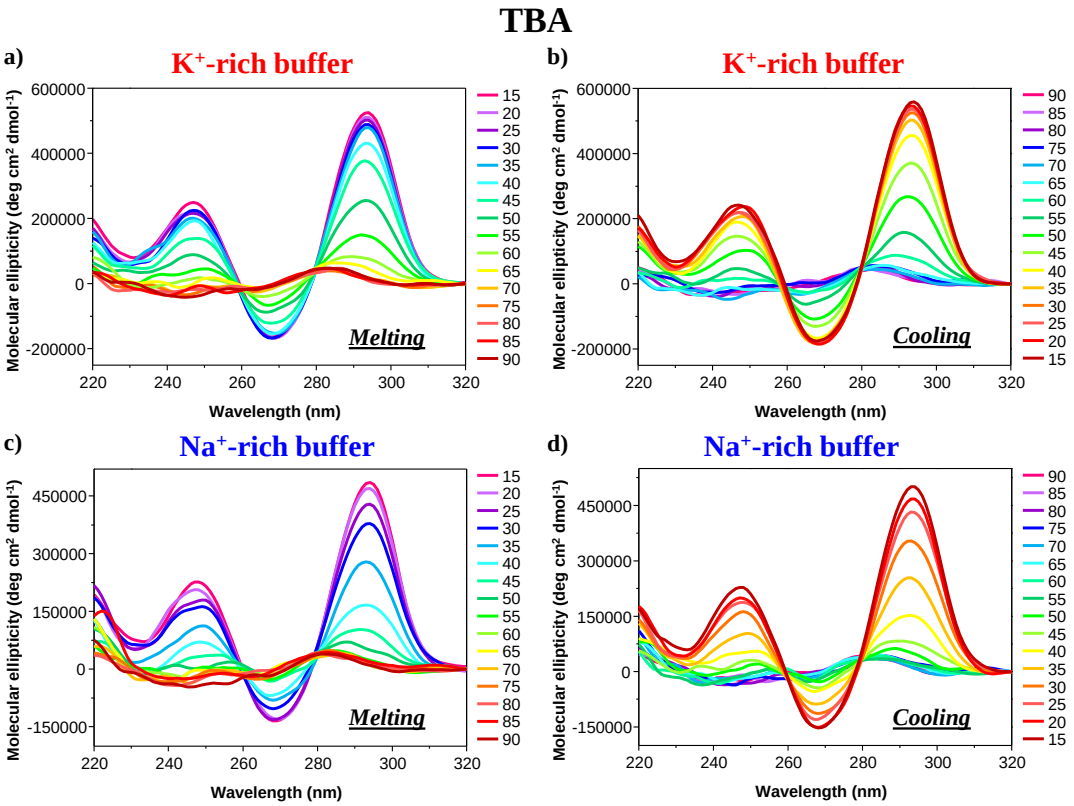

Figure S23. Overlapped CD spectra of **TBA** recorded every 5 °C during the melting (**a**, **c**) and cooling processes (**b**, **d**) in both the selected K^+- (**a**, **b**) and Na^+-rich (**c**, **d**) buffer solutions.

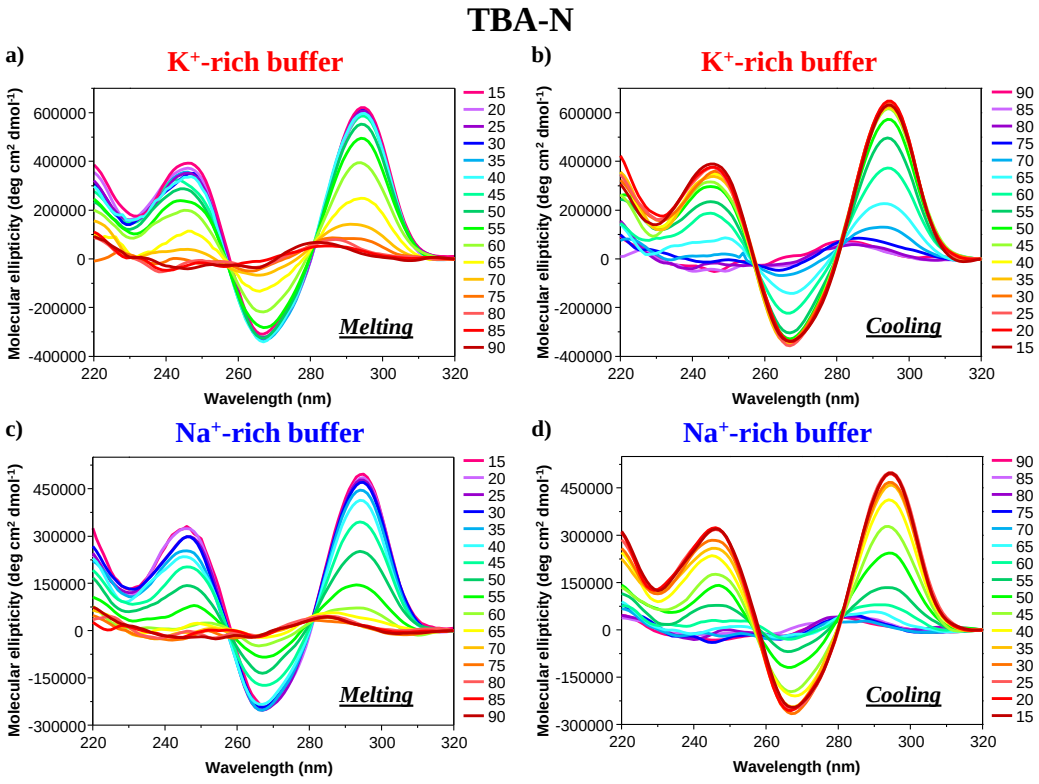

Figure S24. Overlapped CD spectra of **TBA-N** recorded every 5 °C during the melting (**a**, **c**) and cooling processes (**b**, **d**) in both the selected K^+- (**a**, **b**) and Na^+-rich (**c**, **d**) buffer solution.

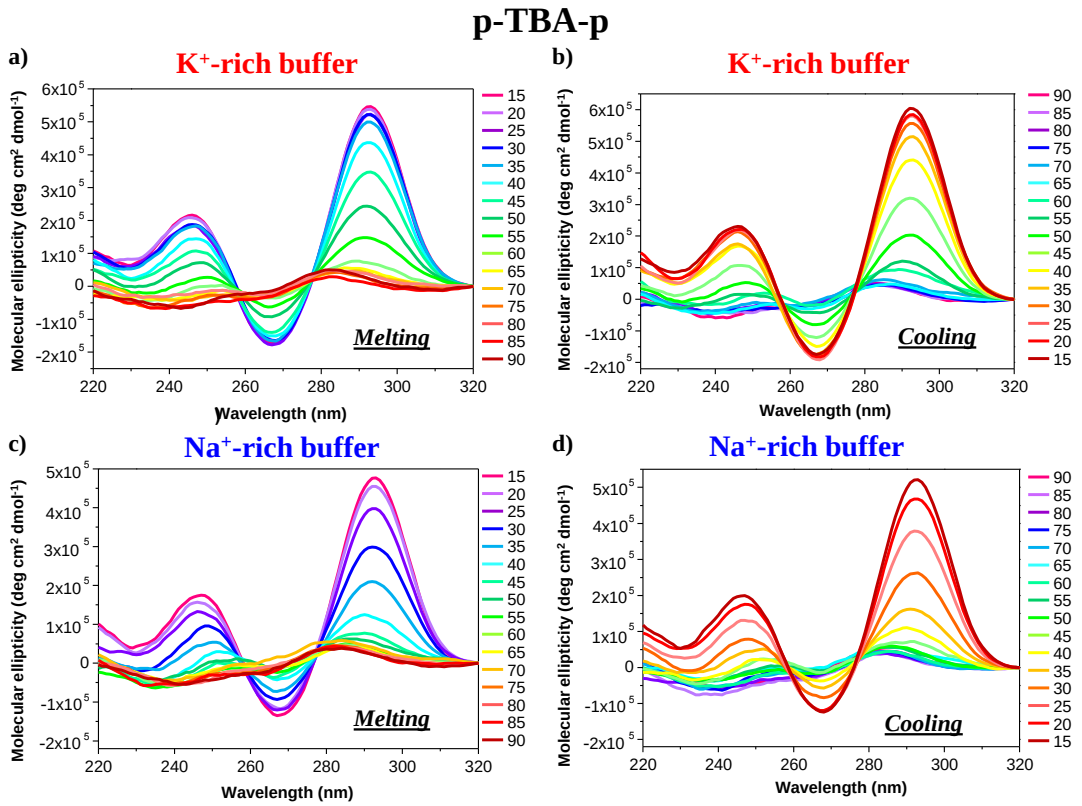

Figure S25. Overlapped CD spectra of **p-TBA-p** recorded every 5 °C during the melting (**a**, **c**) and cooling processes (**b**, **d**) in both the selected K^+- (**a**, **b**) and Na^+-rich (**c**, **d**) buffer solutions.

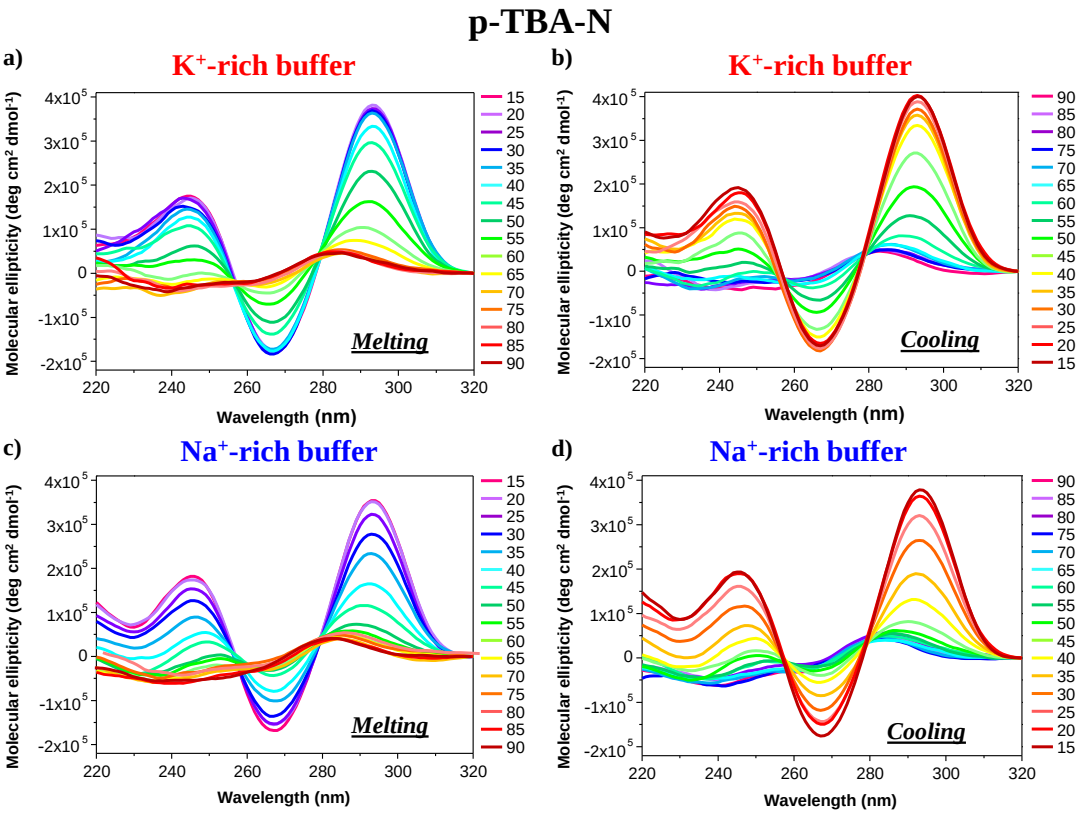

Figure S26. Overlapped CD spectra of **p-TBA-N** recorded every 5 °C during the melting (**a**, **c**) and cooling processes (**b**, **d**) in both the selected K^+- (**a**, **b**) and Na^+-rich (**c**, **d**) buffer solutions.

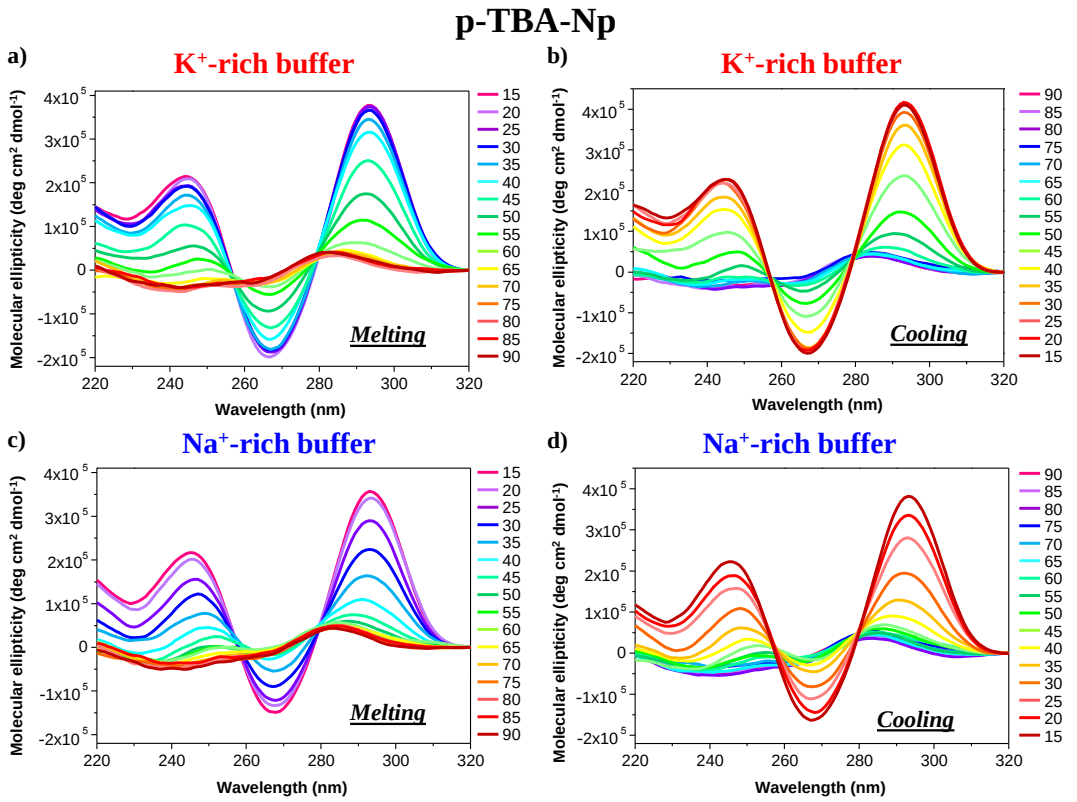

Figure S27. Overlapped CD spectra of **p-TBA-Np** recorded every 5 °C during the melting (**a**, **c**) and cooling processes (**b**, **d**) in both the selected K^+- (**a**, **b**) and Na^+-rich (**c**, **d**) buffer solutions.

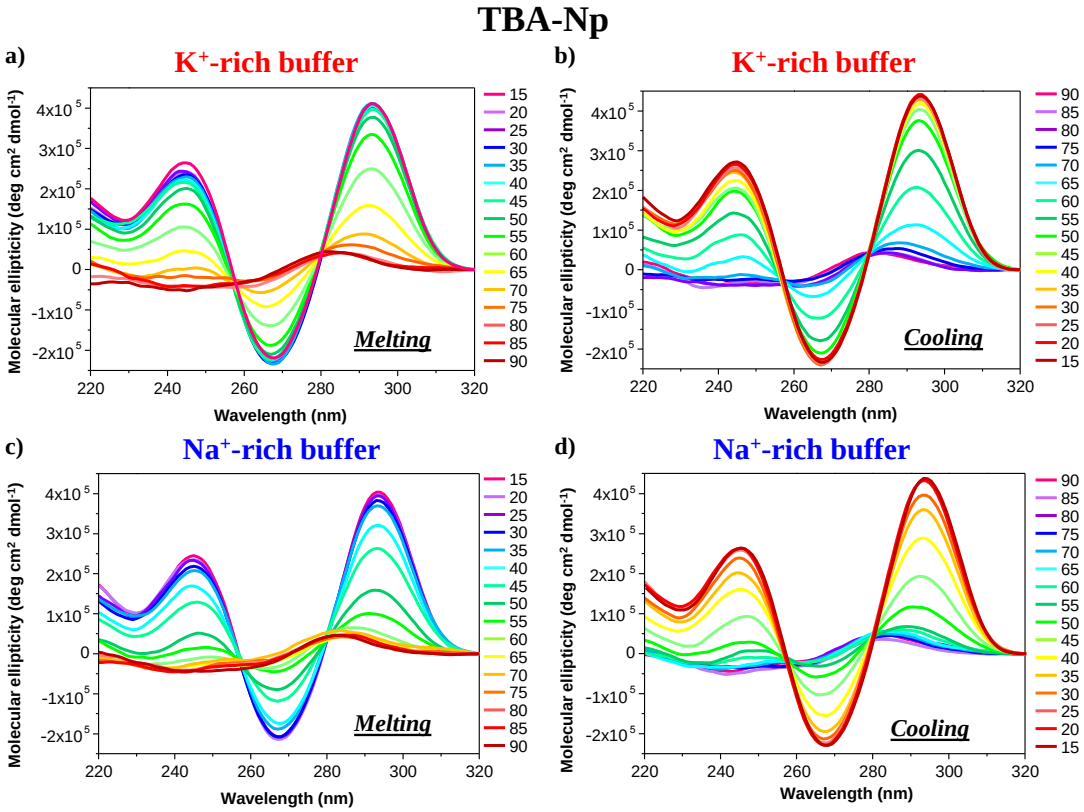

Figure S28. Overlapped CD spectra of **TBA-Np** recorded every 5 °C during the melting (**a**, **c**) and cooling processes (**b**, **d**) in both the selected K^+- (**a**, **b**) and Na^+-rich (**c**, **d**) buffer solutions.

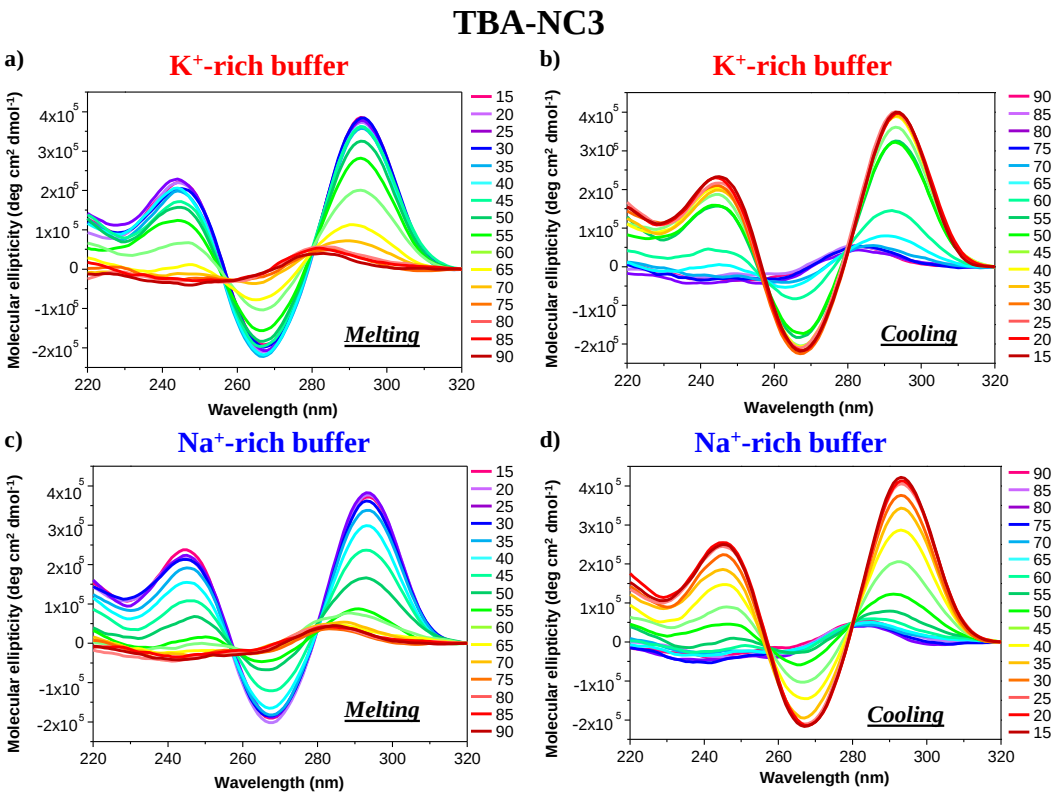

Figure S29. Overlapped CD spectra of **TBA-NC3** recorded every 5 °C during the melting (**a**, **c**) and cooling processes (**b**, **d**) in both the selected K^+- (**a**, **b**) and Na^+-rich (**c**, **d**) buffer solutions.

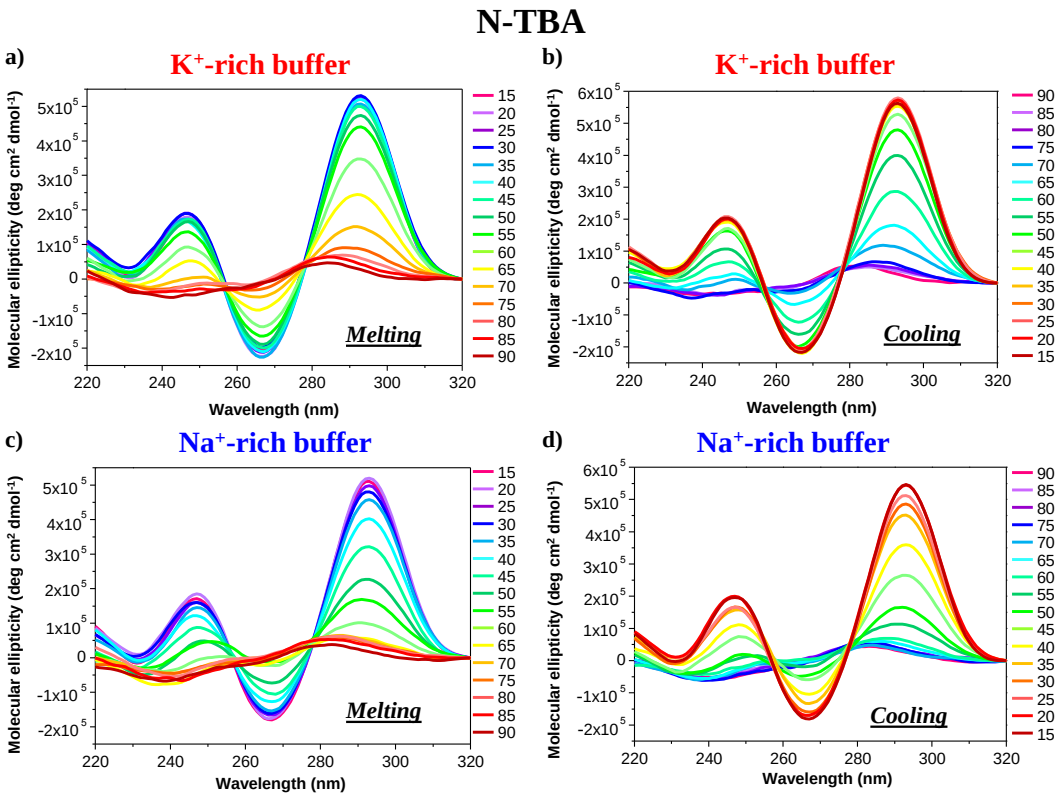

Figure S30. Overlapped CD spectra of **N-TBA** recorded every 5 °C during the melting (**a**, **c**) and cooling processes (**b**, **d**) in both the selected K^+- (**a**, **b**) and Na^+-rich (**c**, **d**) buffer solutions.

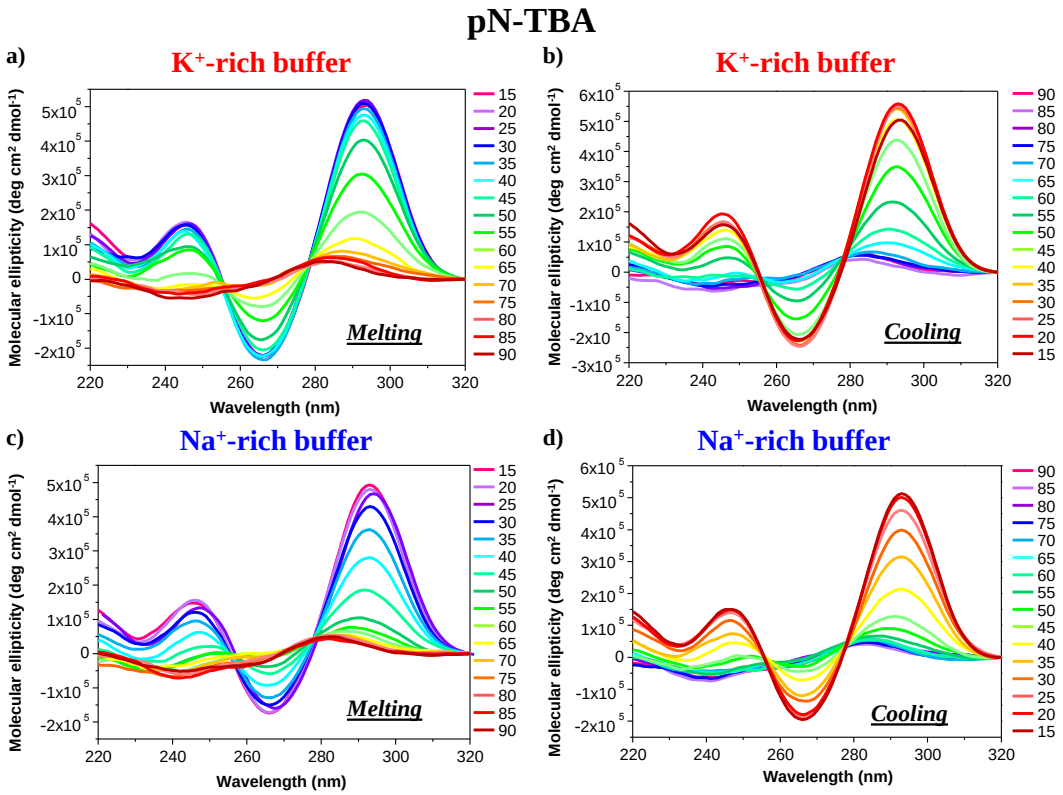

Figure S31. Overlapped CD spectra of **pN-TBA** recorded every 5 °C during the melting (**a**, **c**) and cooling processes (**b**, **d**) in both the selected K^+- (**a**, **b**) and Na^+-rich (**c**, **d**) buffer solutions.

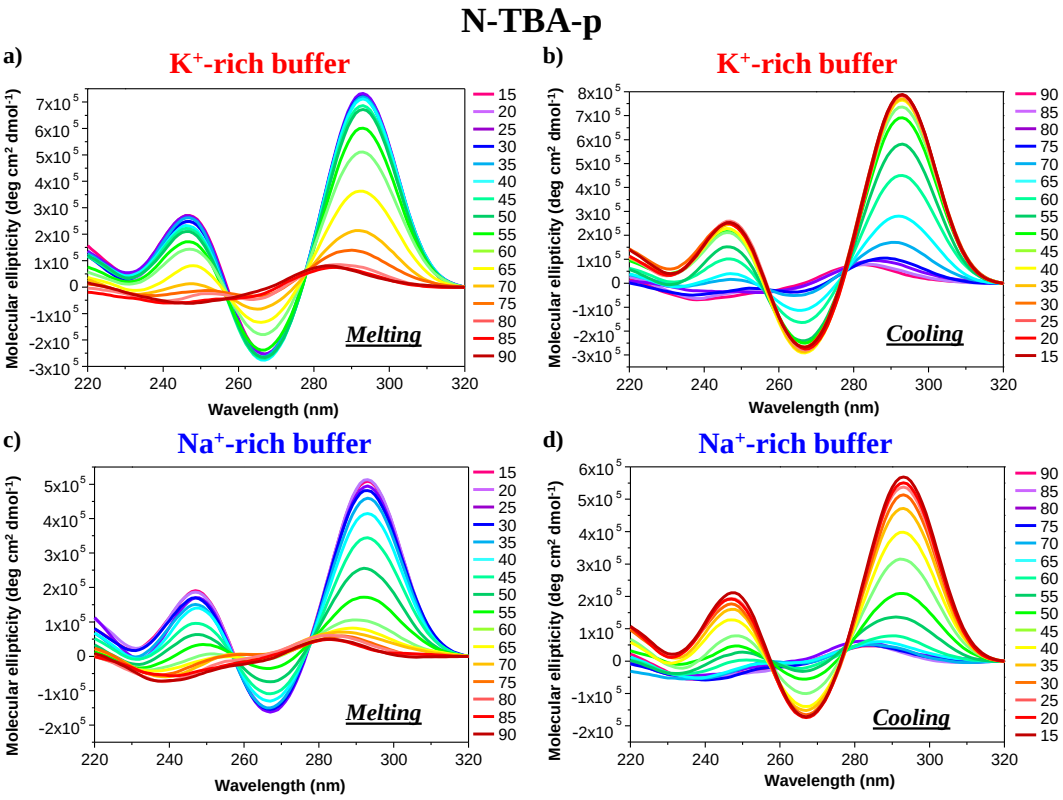

Figure S32. Overlapped CD spectra of **N-TBA-p** recorded every 5 °C during the melting (**a**, **c**) and cooling processes (**b**, **d**) in both the selected K^+- (**a**, **b**) and Na^+-rich (**c**, **d**) buffer solutions.

Aptamer	K^+-rich buffer			Na^+-rich buffer		
	ΔH^0 (kJ mol^{-1})	ΔS^0 (kJ mol^{-1} K^{-1})	ΔG^0_{298K} (kJ mol^{-1})	ΔH^0 (kJ mol^{-1})	ΔS^0 (kJ mol^{-1} K^{-1})	ΔG^0_{298K} (kJ mol^{-1})
TBA	-166.3 ± 2.6	-0.51 ± 0.01	-13.6 ± 0.2	-146.6 ± 3.2	-0.47 ± 0.01	-5.7 ± 0.3
TBA-N	-179.1 ± 4.5	-0.53 ± 0.01	-20.5 ± 0.5	-159.0 ± 1.6	-0.49 ± 0.01	-13.0 ± 0.3
p-TBA-p	-155.5 ± 1.1	-0.49 ± 0.01	-10.4 ± 0.1	-136.9 ± 7.0	-0.45 ± 0.02	-3.8 ± 0.5
TBA-Np	-183.9 ± 4.6	-0.55 ± 0.01	-20.4 ± 0.2	-152.0 ± 17.2	-0.47 ± 0.05	-11.2 ± 1.3
p-TBA-N	-151.9 ± 8.9	-0.47 ± 0.03	-13.2 ± 0.9	-122.7 ± 5.7	-0.39 ± 0.02	-5.7 ± 0.5
p-TBA-Np	-153.5 ± 4.8	-0.48 ± 0.01	-11.1 ± 0.9	-126.5 ± 4.2	-0.41 ± 0.01	-3.0 ± 0.1
TBA-NC3	-188.0 ± 7.1	-0.56 ± 0.02	-20.0 ± 1.1	-165.8 ± 2.5	-0.51 ± 0.01	-12.5 ± 0.2
N-TBA	-166.8 ± 6.4	-0.49 ± 0.02	-20.2 ± 0.1	-131.4 ± 3.1	-0.41 ± 0.01	-9.8 ± 0.2
pN-TBA	-167.1 ± 1.6	-0.51 ± 0.01	-16.1 ± 0.1	-135.8 ± 8.0	-0.43 ± 0.03	-7.5 ± 0.5
N-TBA-p	-152.3 ± 5.4	-0.45 ± 0.02	-18.8 ± 0.3	-137.2 ± 1.5	-0.42 ± 0.01	-11.1 ± 0.2

Table S4. Standard thermodynamic parameters as derived from van't Hoff analysis (ΔH^0, ΔS^0 and ΔG^0 calculated at 298 K) for the unfolding process of unmodified TBA and its modified analogues, monitored by CD spectroscopy in the selected buffer solutions.

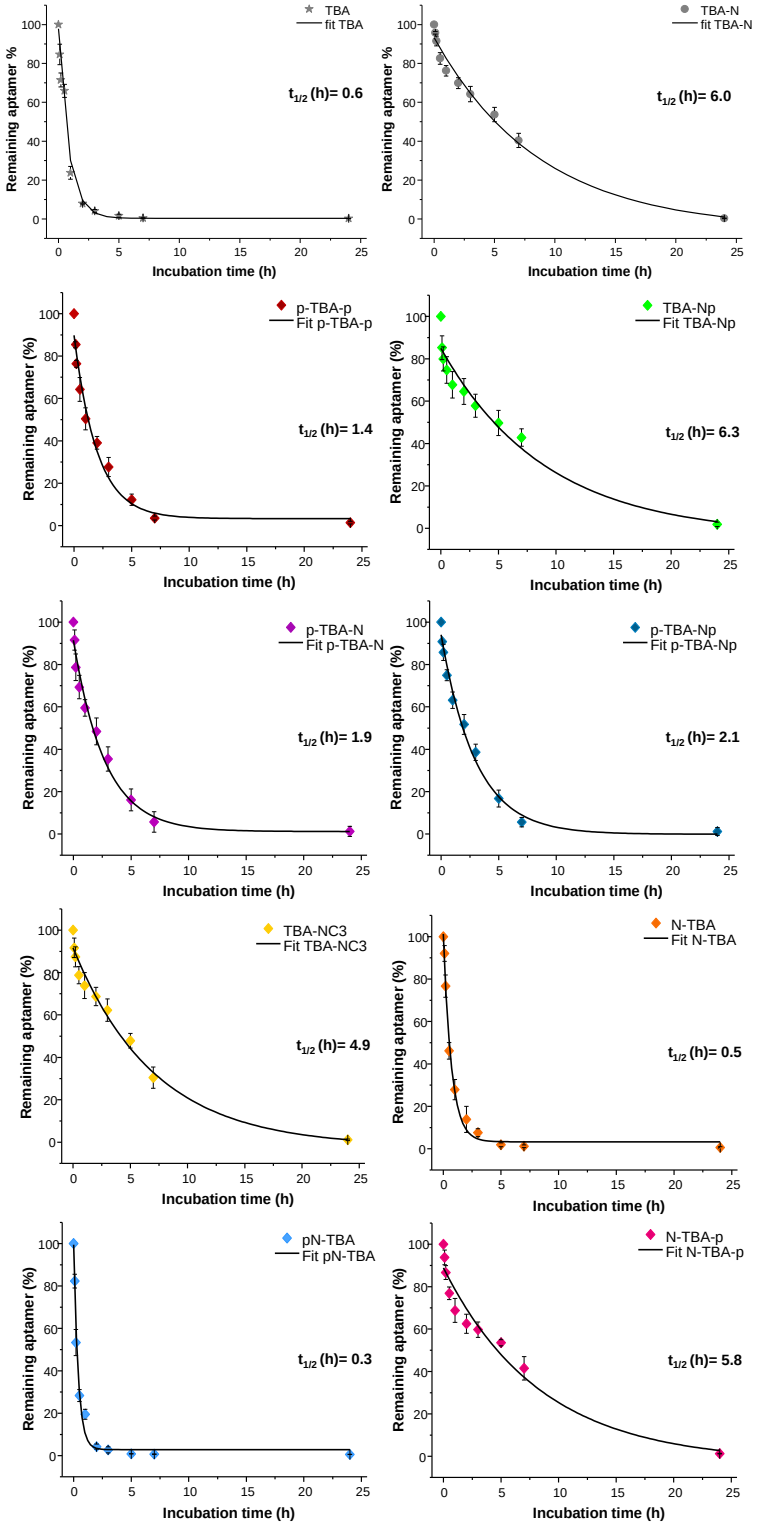

Figure S33. Enzymatic resistance experiments performed on the here investigated TBA analogues, as monitored by denaturing 20% PAGE up to 24 h. Intensity of each oligonucleotide band on the gel is expressed as percentage of the remaining aptamer with respect to the initial one (untreated oligonucleotide) for all the analyzed time points. Data are reported as mean values ± SD (error bars) for three independent determinations. Obtained values were also fitted with an equation for first order kinetics (lines) allowing the calculation of the half-life in serum of each aptamer ($t_{1/2}$).

Aptamer	Anticoagulant activity	Improved potency vs. TBA
TBA	1.5 ± 0.2	-
TBA-N	2.1 ± 0.5	1.4
p-TBA-p	5.2 ± 0.5	3.5
TBA-Np	5.0 ± 0.6	3.3
p-TBA-N	2.0 ± 0.2	1.3
p-TBA-Np	9.7 ± 1.0	6.5
TBA-NC3	3.5 ± 1.0	2.3
N-TBA	6.9 ± 0.2	4.6
pN-TBA	7.0 ±1.7	4.7
N-TBA-p	11.1 ± 0.5	7.4
cycTBA II	8.5 ± 0.6	5.7
TBA-NNp/DDp	5.4 ± 0.5	3.6
TBA-Np/Np	4.4 ± 0.6	2.9
p-TBA-Np 1:10	22.6 ± 0.5	15.1
N-TBA-p 1:10	26.4 ± 0.9	17.6

Table S5. Anticoagulant activity of the different aptamers here studied expressed as the ratio between the coagulation rate in the presence of both thrombin and each tested oligonucleotide and in the only presence of the protein. In all cases, data are referred to experiments in which a 1:5 thrombin/aptamer molar ratio was used, with the exception of the latter two in the series, where a 1:10 ratio was used (*cfr*. Figure S34). All the values are reported as mean values ± SD of at least three independent measurements.

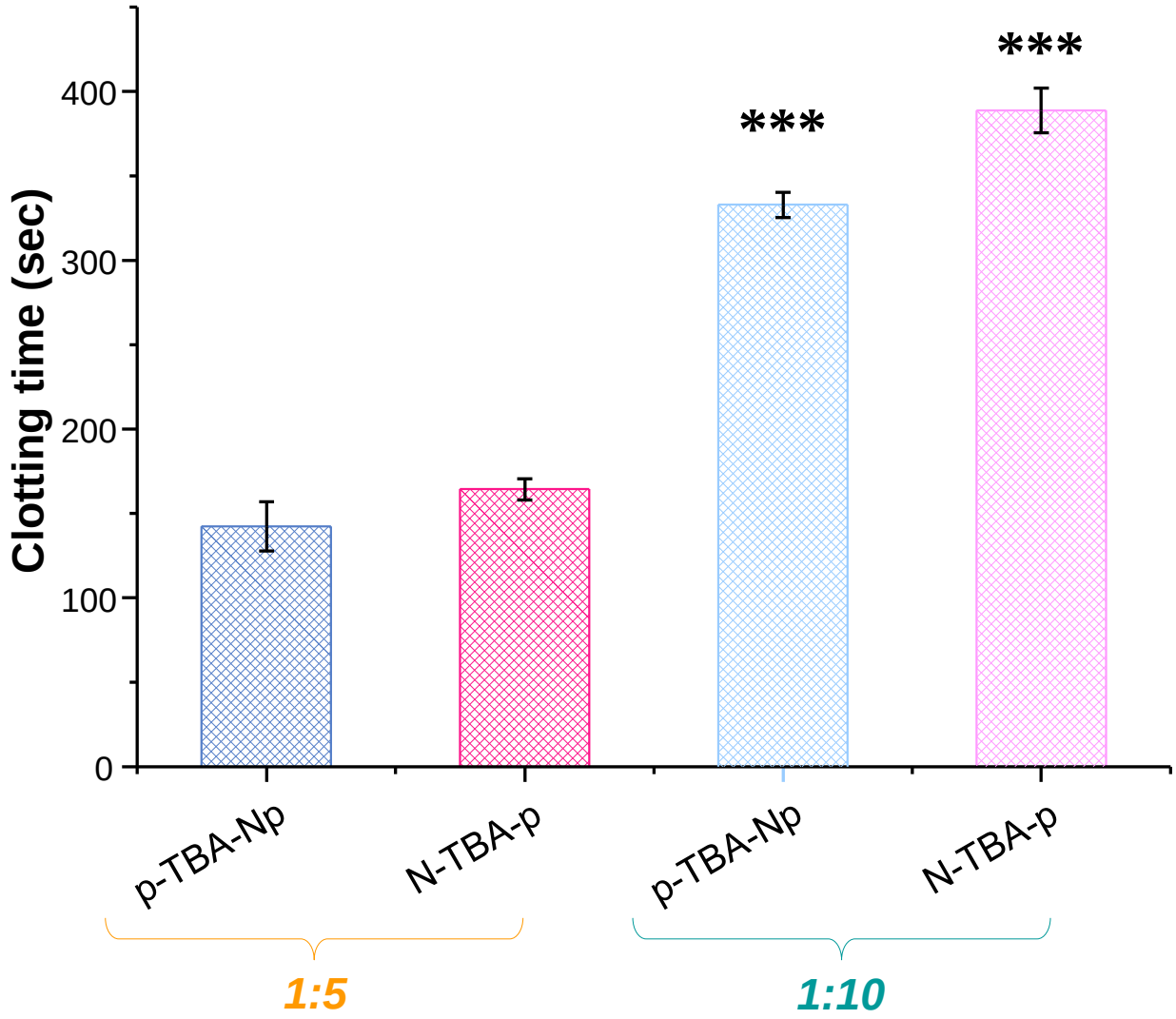

Figure S34. Fibrinogen clotting times (sec) as determined from the maxima of the second derivative of UV-monitored scattering curves for **p-TBA-Np** and **N-TBA-p** at 1:5 and 1:10 thrombin:aptamer molar ratio (fibrinogen: 1.8 mg/mL, α-thrombin: 5 nM). Data are reported as mean values ± SE (error bars) for multiple determinations. Statistical significance was assessed by using Student's t-test: *p < 0.1, **p < 0.05 or ***p < 0.01 *vs.* the same compound at 1:5 molar ratio.

Figure S35. Reverse phase C18 HPLC and MALDI-TOF MS analysis of **p-TBA-p**:

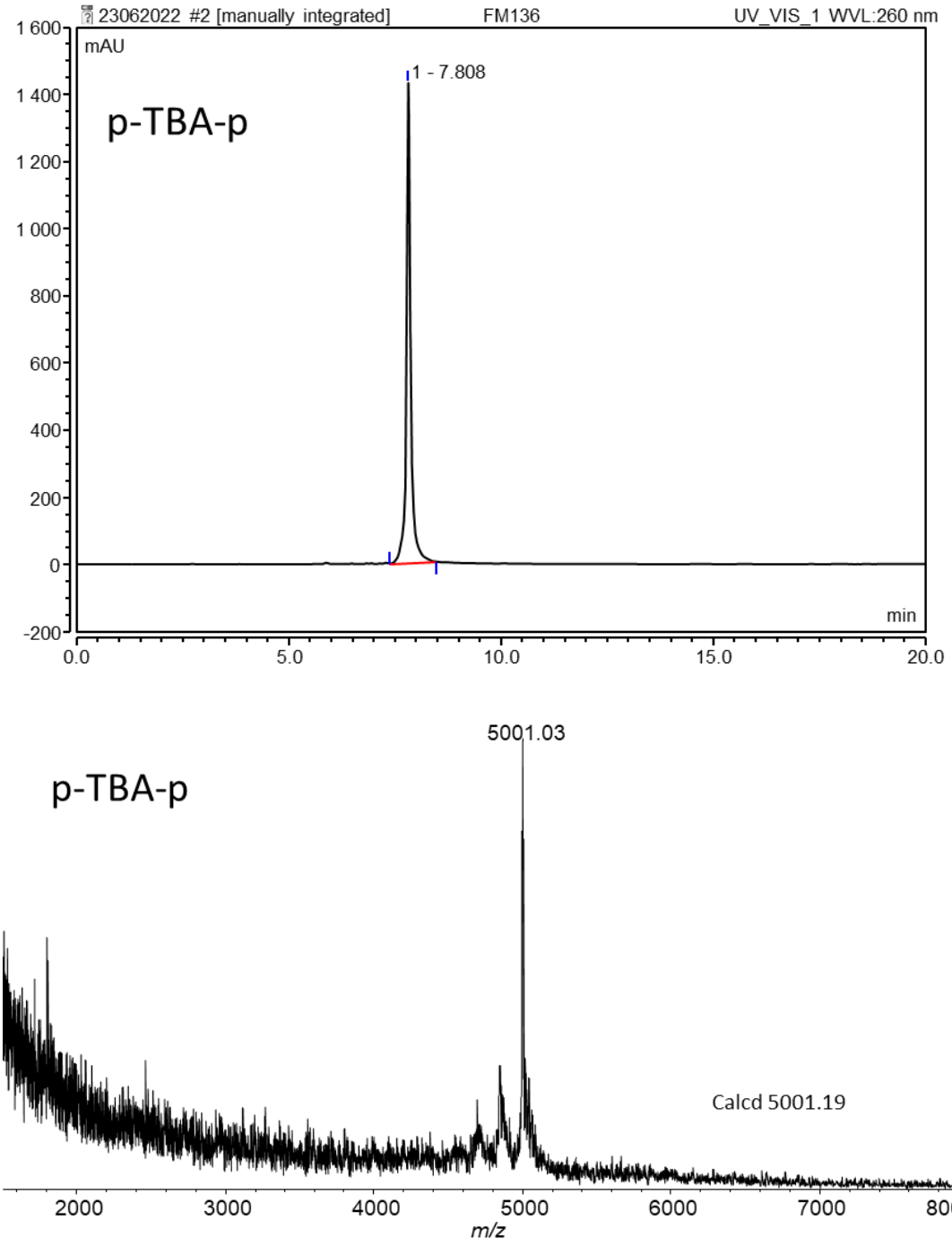

Figure S36. Reverse phase C18 HPLC and MALDI-TOF MS analysis of **TBA-Np**:

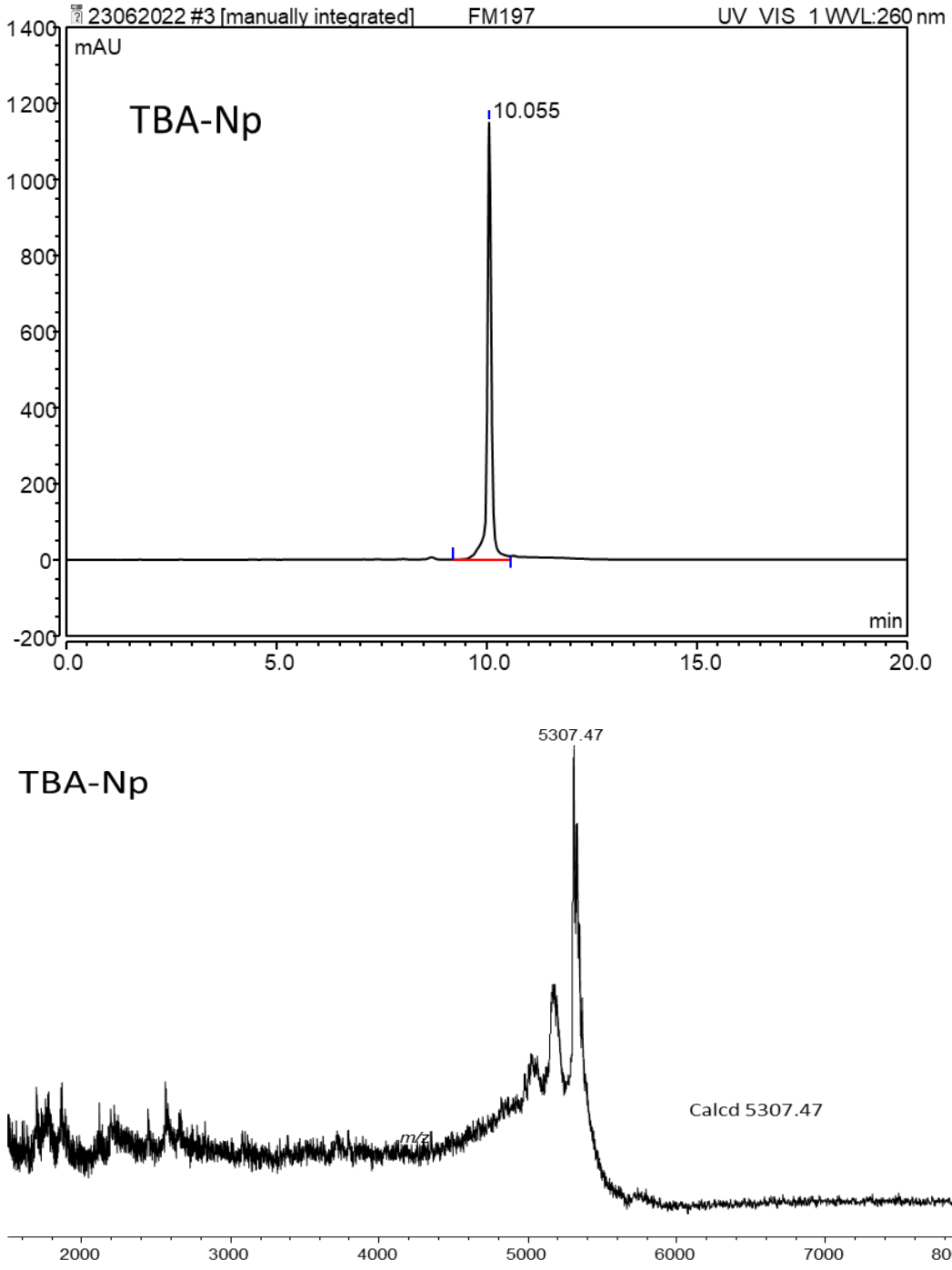

Figure S37. Reverse phase C18 HPLC and MALDI-TOF MS analysis of **p-TBA-N**:

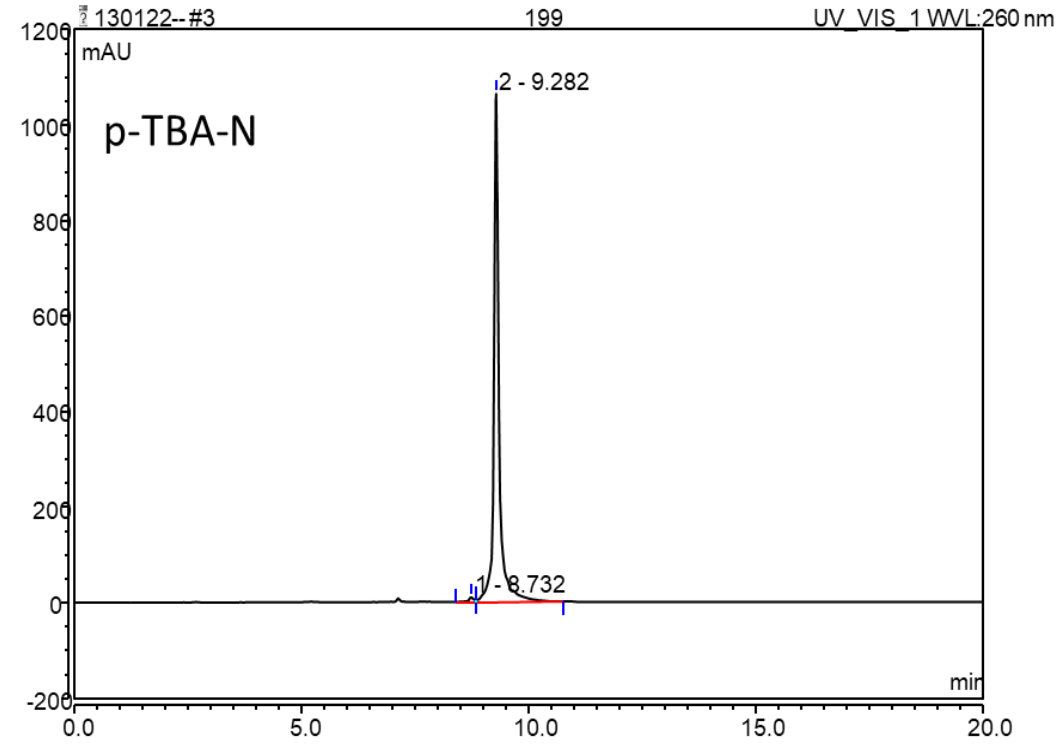

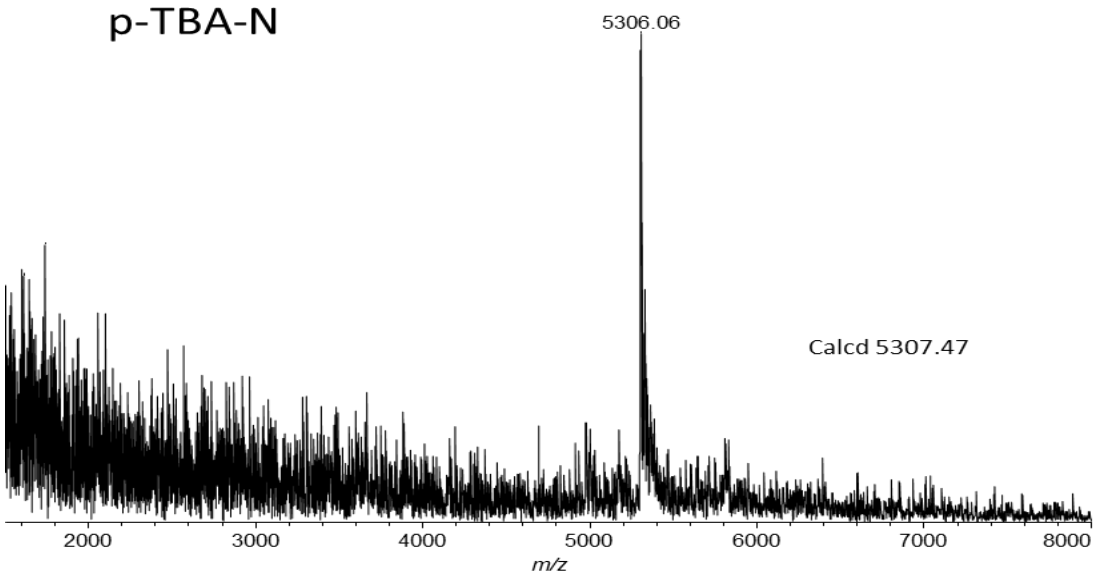

Figure S38. Reverse phase C18 HPLC and MALDI-TOF MS analysis of **p-TBA-Np**:

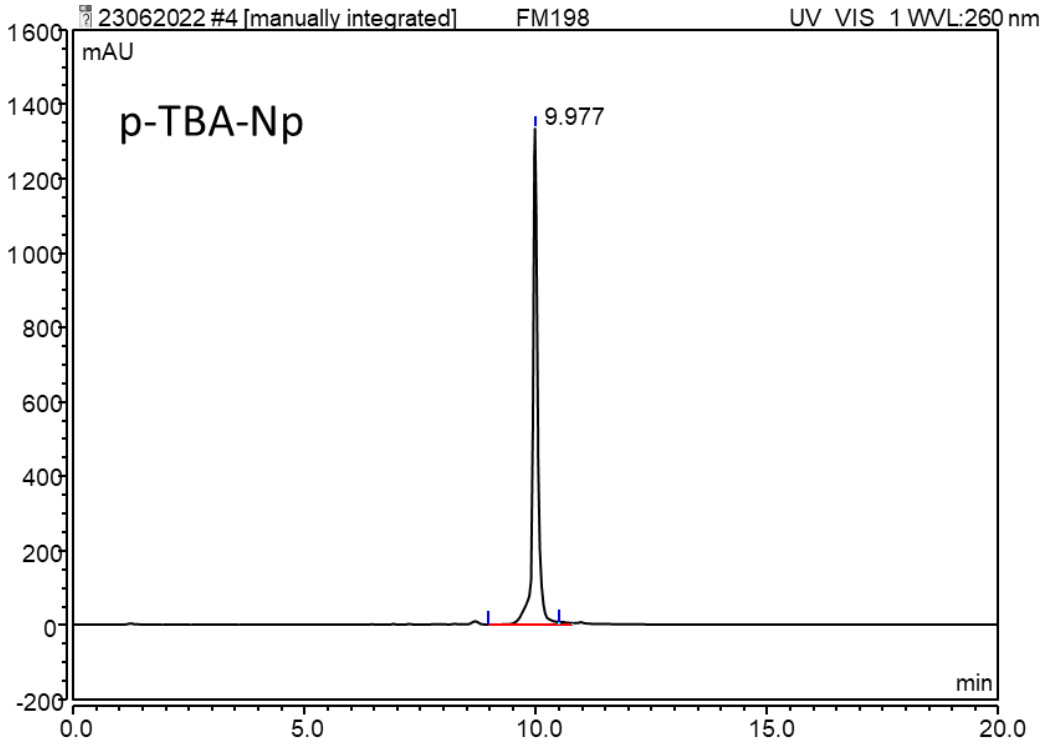

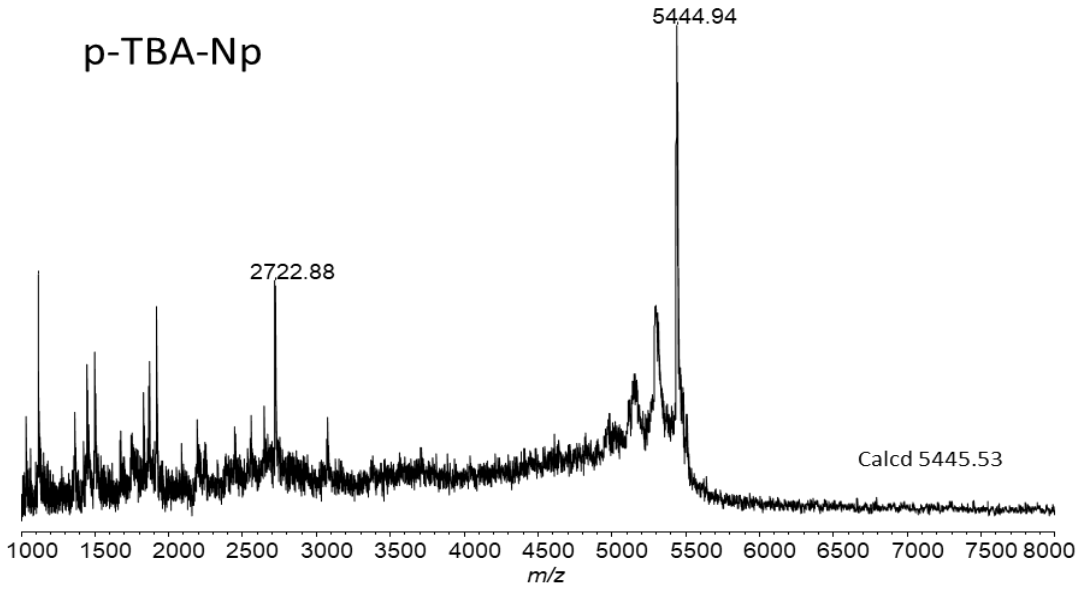

Figure S39. Reverse phase C18 HPLC and MALDI-TOF MS analysis of **TBA-NC3**:

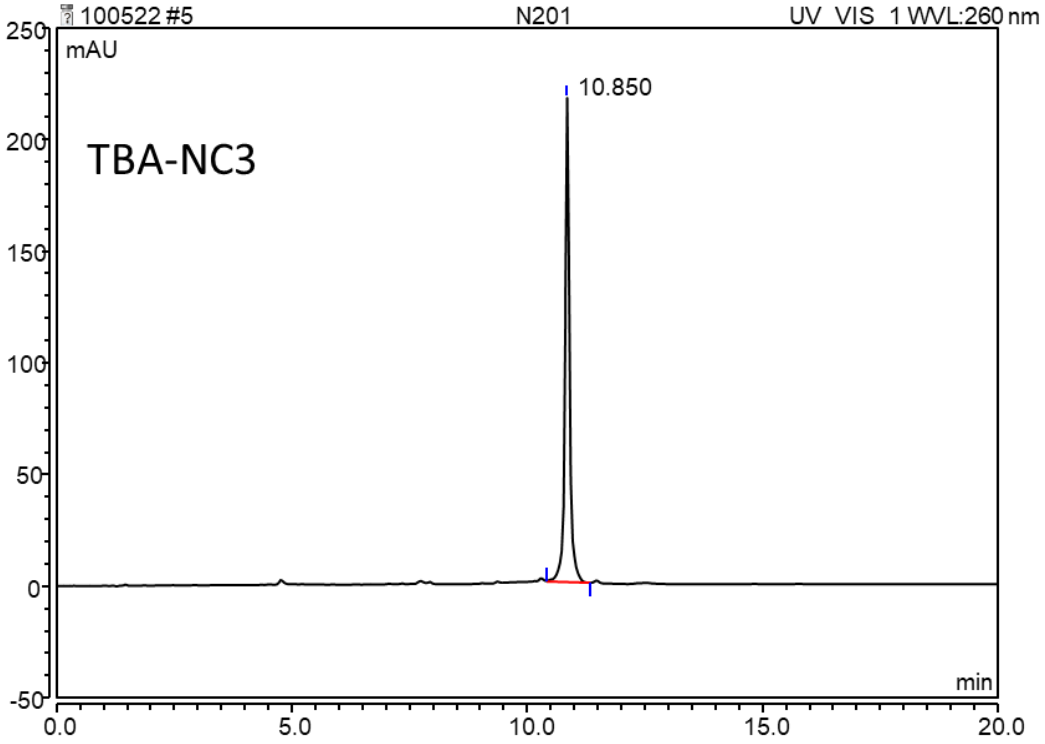

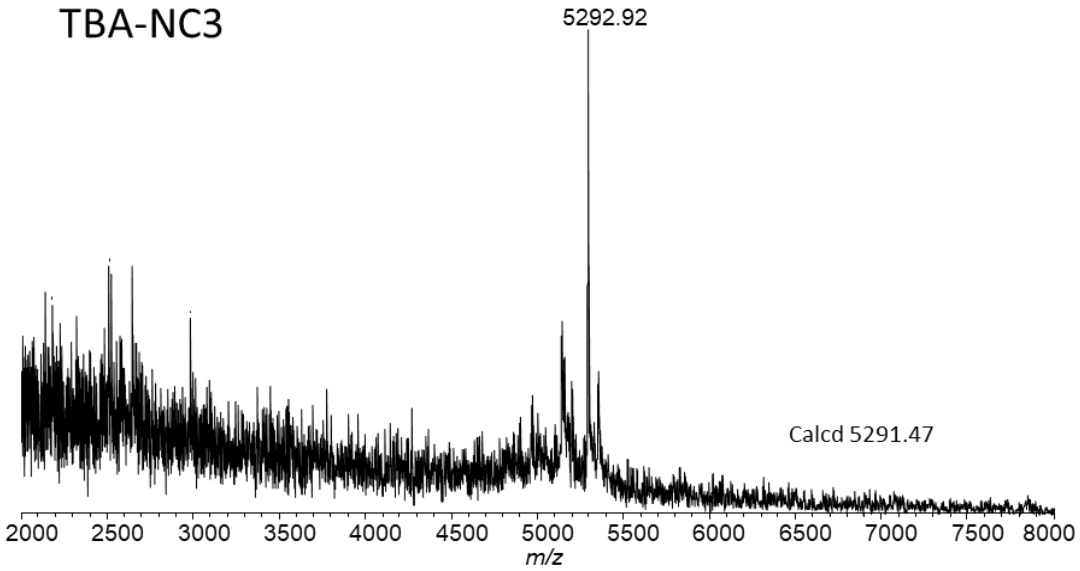

Figure S40. Reverse phase C18 HPLC and MALDI-TOF MS analysis of **N-TBA**:

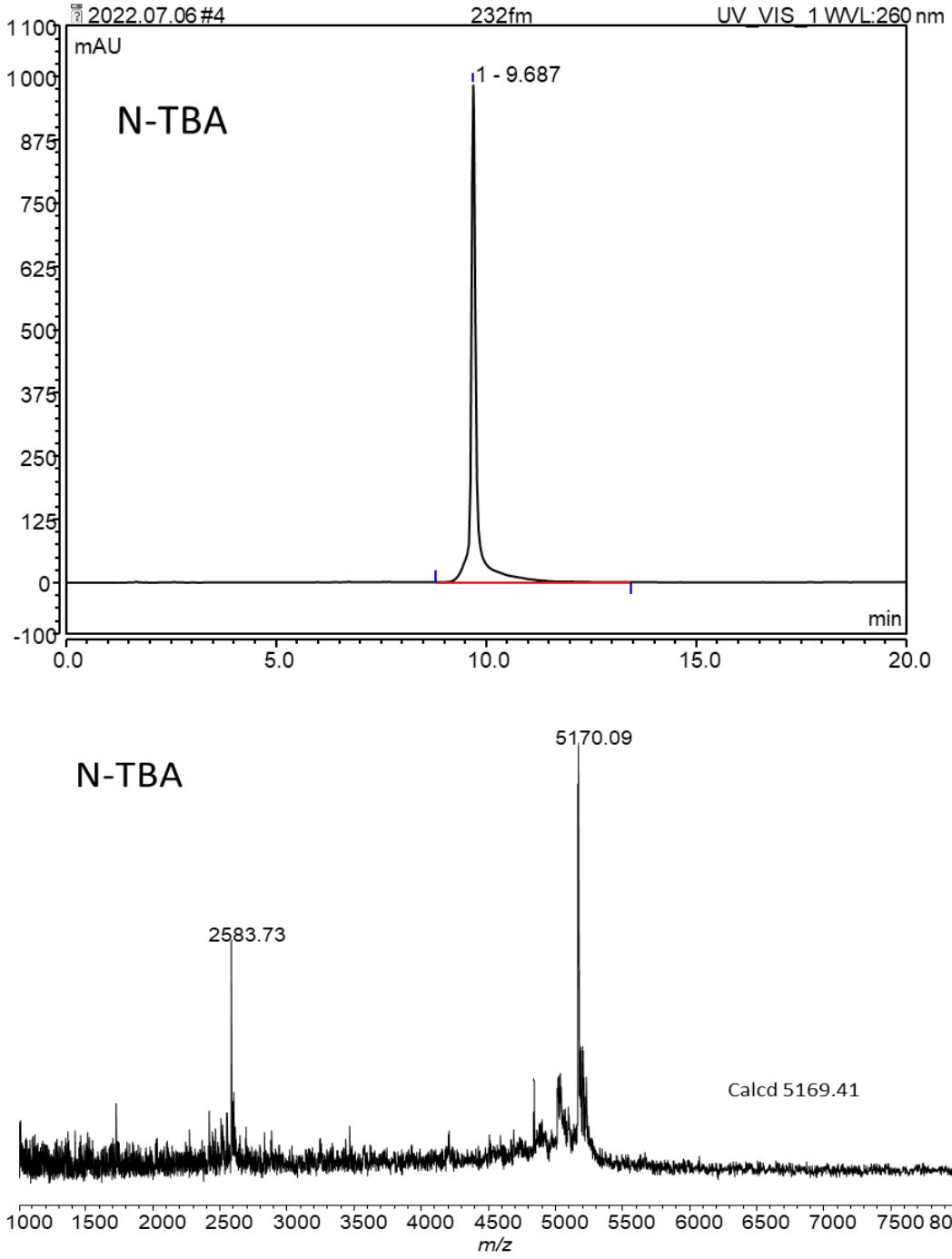

Figure S41. Reverse phase C18 HPLC and MALDI-TOF MS analysis of **pN-TBA**:

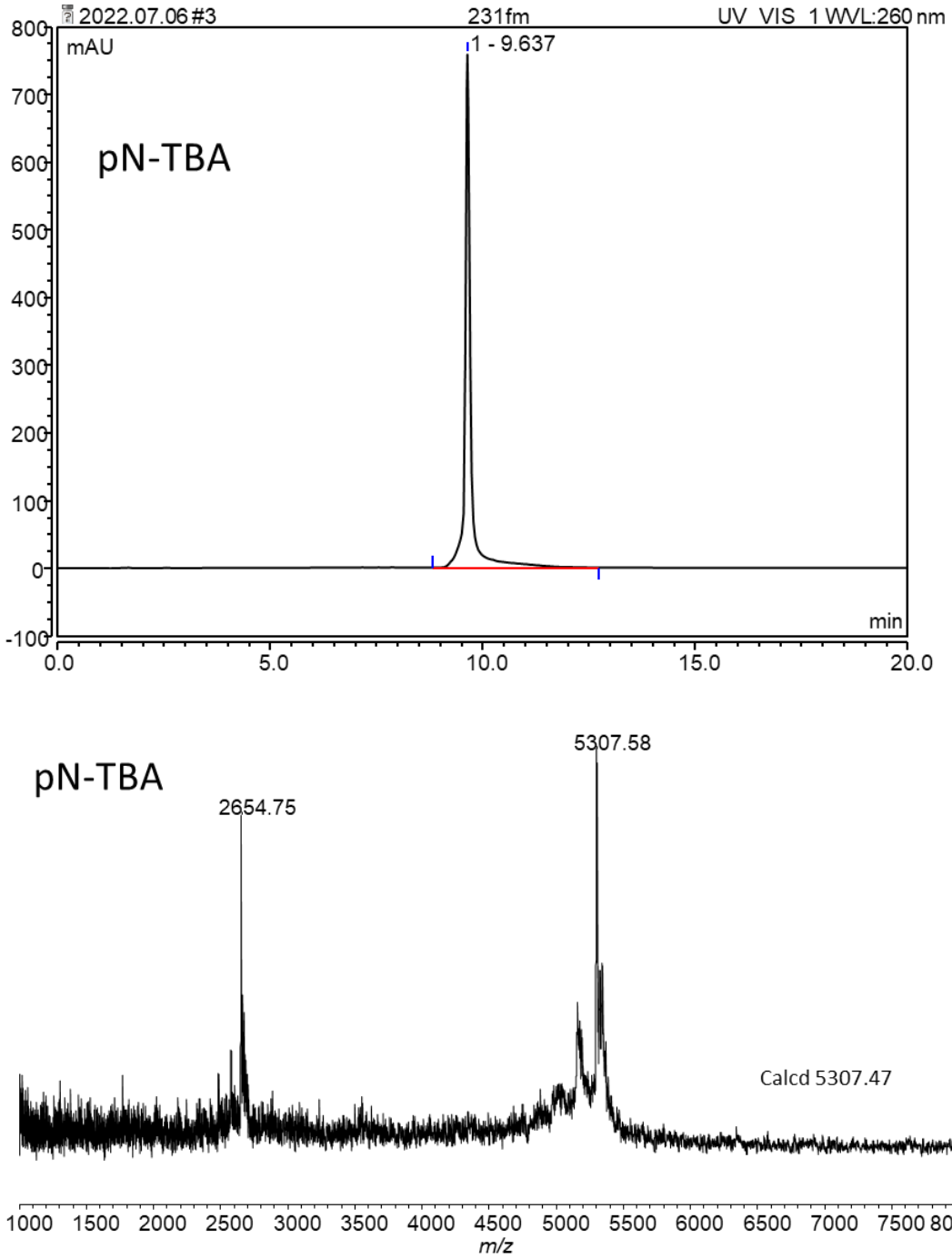

Figure S42. Reverse phase C18 HPLC and MALDI-TOF MS analysis of **N-TBA-p**:

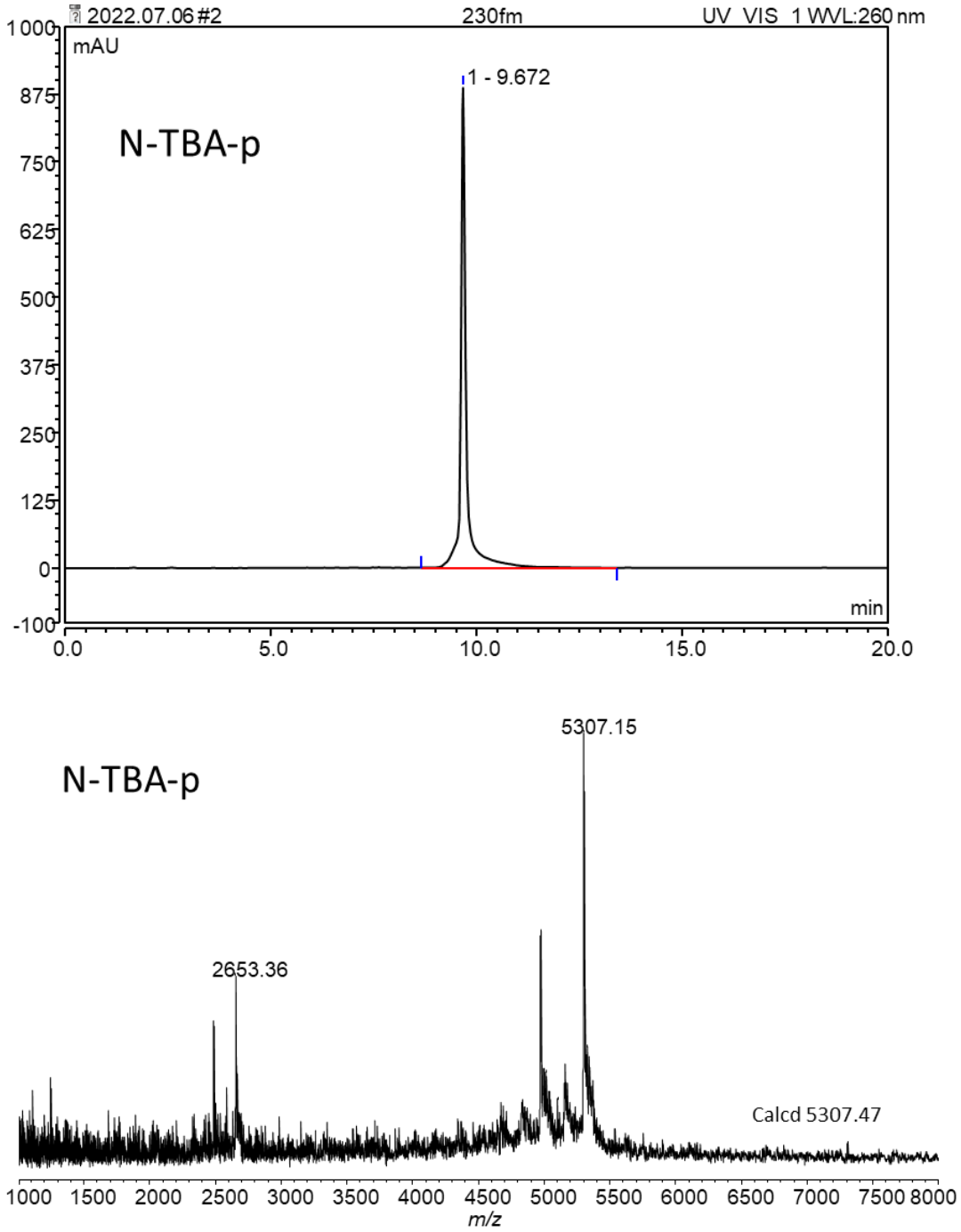

References

[1] A.I. Karsisiotis, N.M.A. Hessari, E. Novellino, G.P. Spada, A. Randazzo, M. Webba da Silva, Topological characterization of nucleic acid G-quadruplexes by UV absorption and circular dichroism, Angew. Chem. - Int. Ed. Eng. 50 (2011) 10645–10648. doi:10.1002/anie.201105193.